Cal Poly SuPER System Simulink Model and Status and Control System

A Thesis
Presented to the Faculty of
California Polytechnic State University,
San Luis Obispo

In Partial Fulfillment
of the Requirements for the Degree of
Master of Science in Electrical Engineering

by
Tyler Sheffield
April 2007

Authorization for Reproduction of Master's Thesis

I grant permission for the reproduction of this thesis in its entirety or any of its parts, without further authorization from me.

Signature (Tyler Sheffield)

Date

Approval

Title: Cal Poly SuPER System Simulink Model and Status and Control System

Author: Tyler Sheffield

Date Submitted: 25th April, 2007

Dr. James Harris
--------------------------- -----------------------------------
Committee Chair Signature

Dr. Ali Shaban
--------------------------- -----------------------------------
Committee Member Signature

Dr. Jim Widmann
--------------------------- -----------------------------------
Committee Member Signature

Abstract

Cal Poly SuPER System Simulink Model and Status and Control System

Tyler Sheffield

The Cal Poly Sustainable Power for Electrical Resources (SuPER) project is developing a solar power DC distribution system designed to intelligently service almost any load that might be needed by a single off-grid household. A prototype has been constructed and tested. This thesis describes the creation of a modular MATLAB Simulink model of the entire system, whose principal components include a PV array, DC-DC buck converter, lead-acid battery, various loads, and a digital status and control subsystem. Also presented is the design of the status and control software, which runs on a Linux PC platform. The Simulink model is validated by comparison to measured prototype responses. Simulations are used to predict SuPER system behavior under various load scenarios, in order to maximize battery life. The simulation will be a valuable development tool for future SuPER advancements.

Table of Contents

List of Figures

List of Tables

Chapter 1: Introduction

1.1 The SuPER Project

The Sustainable Power for Electrical Resources project was born in July of 2005 with Dr. James Harris' white paper describing a durable, low-cost, family owned solar power system [1]. It is intended as a self-contained and self-monitoring off-grid DC system with energy storage capability that will service a wide variety of loads. It was anticipated that development time of the system would be around five years, with the first three years dedicated to research, design, and the building of a prototype system. A goal of SuPER is to demonstrate that the system can extend component life, especially that of the battery, and achieve very low failure rate. It is expected that SuPER will be used by family units in low-income, high-insolation areas of the world.

1.2 Personal Involvement

I first learned about the SuPER project at a presentation made by Dr. James Harris at one of the Friday afternoon sessions of the department's weekly graduate student seminars. Photovoltaic cells are a fascinating technology, and though I knew very little about power generation and distribution it was clear that the call for a digital control system could use some computer engineering expertise. I began meeting with the development team in January 2006, which is about the time construction of the project prototype began.

My contributions to the effort for the first six months of my association with the project consisted largely of support for Eran Tal, working on his thesis [2]. Readers new to SuPER ought to become familiar with Tal’s work, as he led the team in building the first stage of the prototype and provided a foundation for all that has been accomplished since. During this period, I provided some software expertise to the team in doing some C and assembly language programming, as well as managing the Linux development environment on the project computers.

Since Tal graduated in summer 2006 and I took over project leadership, SuPER has been a whirlwind learning experience for me. My educational and professional engineering experiences have largely fallen under the programmable logic, embedded systems and signal processing disciplines. I have never been a power and control systems engineer or a proficient analog circuit designer, yet while working on SuPER I have found a need to be a little bit of each of these in order to reach both personal and team objectives. That is perhaps the most rewarding part of the entire experience. The knowledge gained working on this project has added significant breadth to my pool of engineering resources and tools.

1.3 Solar Power Systems

In section 2.1 of Tal’s 2006 thesis paper [2], he convincingly outlines the case for SuPER; only a summary of his arguments will be presented here. There are multitudinous opinions on whether or not rising global temperatures are directly caused by human activity; regardless of the cause, it is nevertheless a fact that atmospheric carbon dioxide levels, and by extension, temperatures, have been sharply on the rise in the last 25 years [3]. Such changes will have consequences for life on this planet as we know it. SuPER harvests energy from a renewable source, and contributes no direct air pollution to the environment. It is a device designed with the goal of sustainability in mind. It is also intended to be a low-cost system (which will "pay for itself" within a short time of activation [1]) in order to provide advantages to lower income families who have not previously had access to a power generation system. There is no grid infrastructure required as all issues associated with long distance power distribution are removed as costs, obstacles, and energy sinks.

Solar cell technology is becoming increasingly important as an energy source for reasons alluded to above. As a result, it is also becoming a more ubiquitous, better researched, more efficient and more cost-effective technology [4]. The technology is quickly developing into a preferable option among those in SuPER's target market, where cooking, heating and lighting energy needs are largely still provided by fossil-fuels [5].

There are a few commercially-available solar power systems similar in scope to SuPER, such as those manufactured by SunWize (www.sunwize.com). SuPER is an attempt to develop one of these types of systems at much lower cost, and the team anticipates future advancements in technology that will make this possible. This is especially true of solar cell and battery technology. What is unique about SuPER is how it is put together, and perhaps more importantly, why.

In [6] Sharaf and Ul Haque present a DC motor solar power system, along with Simulink models, but there is no storage in the system. In [7] by Chiang, Chang, and Yen a system very similar to SuPER is proposed and prototyped, although it is designed to be a supplement to grid power rather than a replacement. This is the case with many commercial systems. For related reasons the authors are unconcerned with managing individual loads and optimizing battery life. There are countless additional published papers that address a wide variety of other issues with the components that make up SuPER, including, but not limited to, converter topologies, battery state of charge (SOC) measurement, and maximum power point tracking (MPPT) techniques. Most publications referenced by the SuPER team do not propose or demonstrate a system on the scale of the SuPER project.

1.4 Thesis Objectives

The broader focus of the work carried out on this thesis project is the effort to build a reliable, self-monitoring and adjusting 150W solar powered DC plant and distribution system. In these early stages of development, the loads considered are a small television, electric cooler, LEDs for lighting, laptop, and permanent magnet motor. The first seven months of the SuPER team's efforts resulted in a partially complete open-loop system dubbed Phase 0. The white paper mentions the goal of achieving a complete prototype system, Phase 1, within one year of commencement. A few months into project work, the team felt confident in reaching and even exceeding that goal. However, the development of the DC-DC converter, a crucial subsystem, hit a few road blocks. Phase 1 was not achieved by the end of 2006 as expected, nor was it by March 2007 despite the fact that new converter teams came on board in October 2006 and February 2007.

As a result of these hardware setbacks, we were inclined to turn our attention towards other efforts for the time being. The software for the status and control system, written in C, was developed as necessary in preparation for the integration of the converter. The SuPER team also recognized the knowledge that can be gained in simulating such a complex system in computer software, and this thesis presents a complete first generation system model. Such a simulation can reveal what types of load scenarios a 150W panel can support, establish load time and power boundaries, and provide information on how and when to best utilize battery energy storage while maximizing the life of the battery. The simulation will also be critical for making plans for scaling the system up in size (power). The goal of the thesis is to show that a virtual mathematical model of the entire system compares favorably with a prototype system constructed entirely by students (with faculty and staff guidance). Simulink, with its SimPowerSystems model package, is used regularly in industry as a power and control system simulation tool and has been chosen for the SuPER simulation.

Achieving this goal will require characterization of the DC loads and careful study of prototype performance so as to allow proper modeling in Simulink As such, the majority of the work done by the author during fall 2006 and winter 2007 quarters has been in these areas:

1) constructing the Simulink model and simulating the system

2) developing the framework for the prototype status and control system software

3) testing the system operationally under a variety of load conditions

4) characterizing the loads

5) solving both hardware and software bugs that have periodically arisen

6) coordinating and supporting the undergraduate students working on senior projects associated with SuPER

1.5 Document Overview

Chapter two introduces the SuPER system prototype as it existed in the fall of 2006; included is information about the loads which SuPER will power and specifics about the team's approach to battery management, which becomes a very sensitive issue. Some of the requirements for the next generation of the system are presented, which will provide an understanding of what the SuPER team hoped to accomplish by the end of March 2007.

Chapter three provides the details for the software of the prototype's status and control system, the real brains of SuPER. The system consists of a series of sensors which feed data into a laptop computer for computations and convey corresponding output signals to control various components.

Chapter four represents the bulk of the work done by the author, which was the creation of a MATLAB Simulink model of the entire SuPER system. Each part of the model is presented, and design decisions defended.

Chapter five describes through examples how the simulation is used to estimate the optimal control strategies to be put into use with the prototype's control system. A comparison of measurements of the prototype in action and simulation results is made for multiple load scenarios.

The final chapter gives closure to things learned and conclusions determined from the experiences of this thesis work. Recommendations are made for the future as part of a review on problems that have now been neatly defined thanks to the progress made on SuPER in the last six months.

Appendices at the very end of the document are a repository for information pertinent to the success of SuPER but supplementary in nature to this thesis.

Chapter 2: Background

2.1 Phase 0 Prototype

Tal spearheaded the effort throughout the first half of 2006 to assemble the first SuPER system. The resulting system is a completely functional prototype, and the current state of the system is known as the Phase 0 system (Figure 2.1).

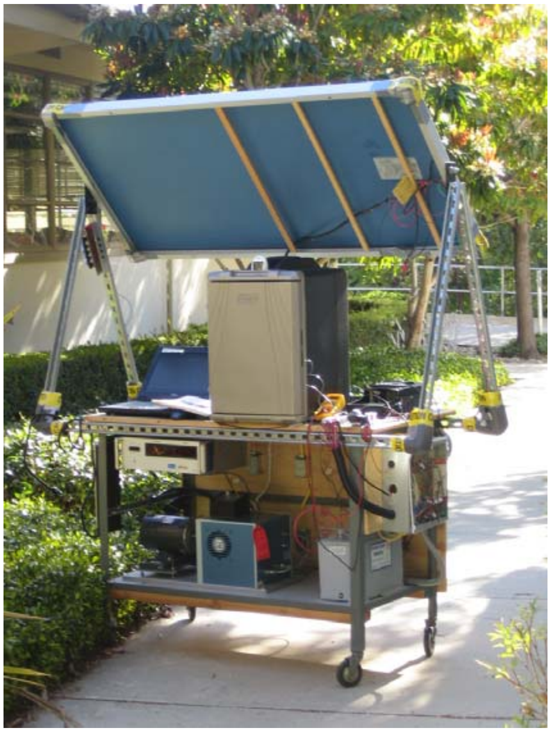

Figure 2.1 - Photo of SuPER Cart, Associated Loads

SuPER consists of a PV array, DC-DC converter, storage battery, and DC loads. Batteries are one of the most expensive components in the system as they cannot be manufactured on campus. Two of the key loads in the system, a water pump and small refrigerator, are intended to be run primarily during hours of peak insolation, but the SuPER team also considers evening lighting to be an essential load. The improvement in safety and reliability of electrical lighting over fossil-fuel consuming sources is worth the additional cost and complexity of including battery storage. Figure 2.2 is the Phase 0 block diagram.

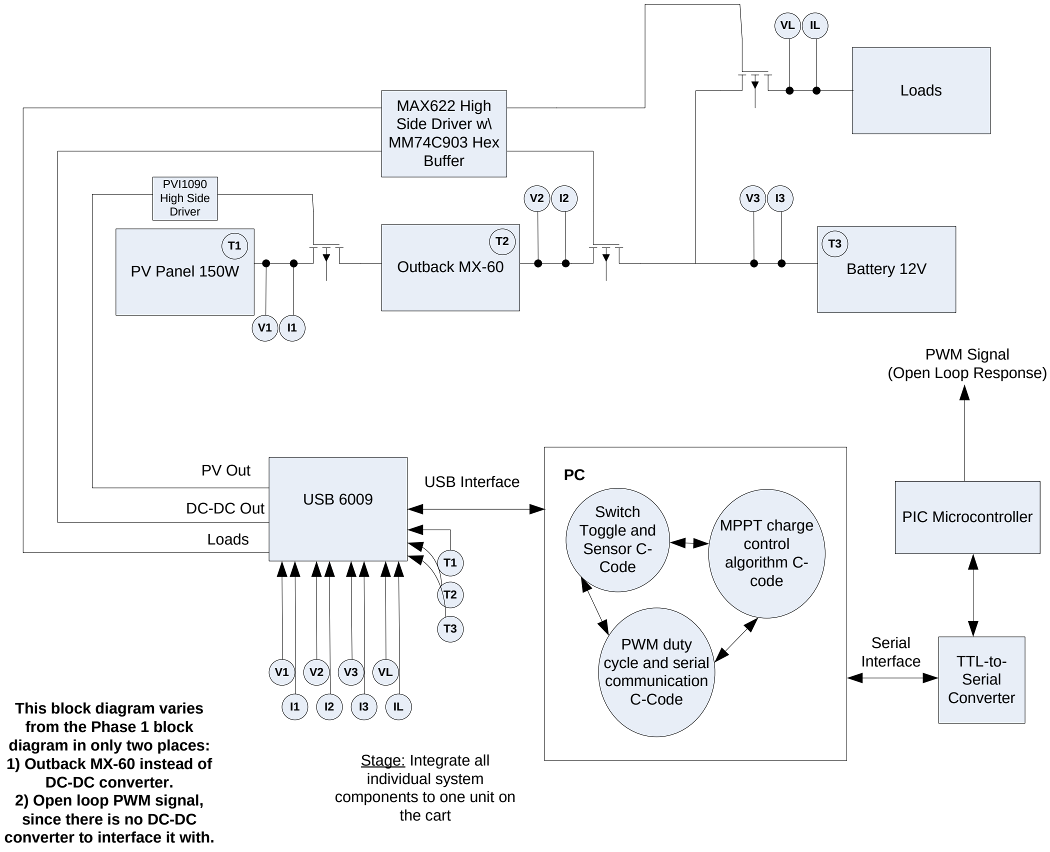

This block diagram varies from the Phase 1 block diagram in only two places:
1) Outback MX-60 instead of DC-DC converter.
2) Open loop PWM signal, since there is no DC-DC converter to interface it with.

Stage: Integrate all individual system components to one unit on the cart

Figure 2.2 - Phase 0 Block Diagram [2]

The Phase 0 system uses the MX60, a high-capacity DC-DC converter manufactured by Outback Power Systems, to buck the voltage level from the PV array to the desired 12V level on the load and battery bus. The MX60 is not simply a converter, but also an MPPT charge controller. This feature has been critical for this early period of prototype development.

2.1.1 Power and Distribution

It was hoped that the Phase 0 system would provide about 400Wh of energy per day. About half of that was earmarked for the 187W DC motor, while the remainder would service the battery and all other loads. However, the motor's *output* rating is 187W. The permanent magnet motor is not 100% efficient, and to produce 187W of power the motor requires more than 240W of input power. In addition, the laptop needs to be running at all times throughout the day and requires at least 240Wh for an eight hour run. As such, the priorities of the Phase 1 control system needed to be reconsidered, and this will be discussed in later chapters.

See Figure 2.3 for the Phase 0/1 power flow diagram. Power consumed by sensor and switch boards, lost in cable and switch resistances, or otherwise unaccounted for and attributed to system losses, is significant and preliminary loss investigations will be presented in chapter five.

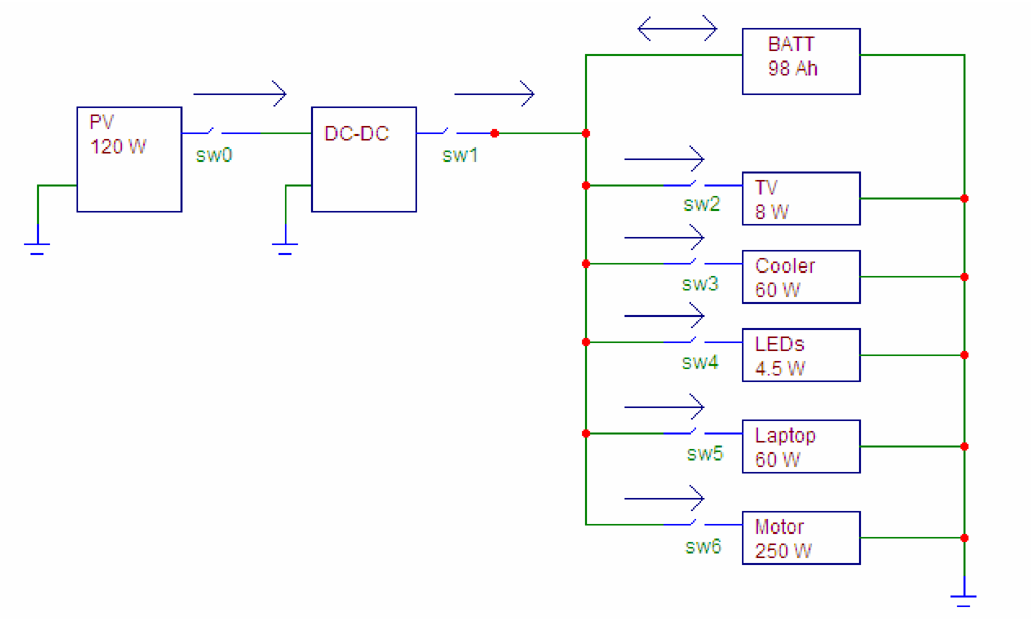

Figure 2.3 – SuPER Power Flow Diagram

During previous work on SuPER, the team had somehow overlooked the problematic issue of high current (which we will call current above five amps) traversing the copper traces on the switch board PCB. This was not realized until motor testing one afternoon. The load torque was increased to about 4 lb·in, which was higher than previously tested values. At this level the motor seeks to draw upwards of seven amps, perhaps eight or nine, depending on the load bus voltage. It turns out that the PCB traces were thick enough only for about five amps, and the increased current caused the traces to heat up and melt the solder joints at the MOSFET. This in turn created a short at the MOSFET terminals. The problem was first noticed when the status system reported a draw of 39A from the battery (due to the newly created short), which would be possible in a scenario with many running loads, but highly abnormal and great cause for alarm in this particular case. In addition, it was unexpected to see such a draw because some measure of protection had been expected from the circuit breakers in the breaker box. However, the team failed to account for the slow response of breakers to negotiating currents above breaker ratings. Breakers do not, in fact, mimic fuses in functionality. Their response instead obeys the tripping time curve seen in Figure 2.4. Thus, for the 30A breaker in use on the hot battery line, a 39A draw is just under 130% of rated current. At that level, it would have taken one minute for the breaker to trip. It was never given a chance as the problem was discovered and the system shut down manually in a matter of a few seconds.

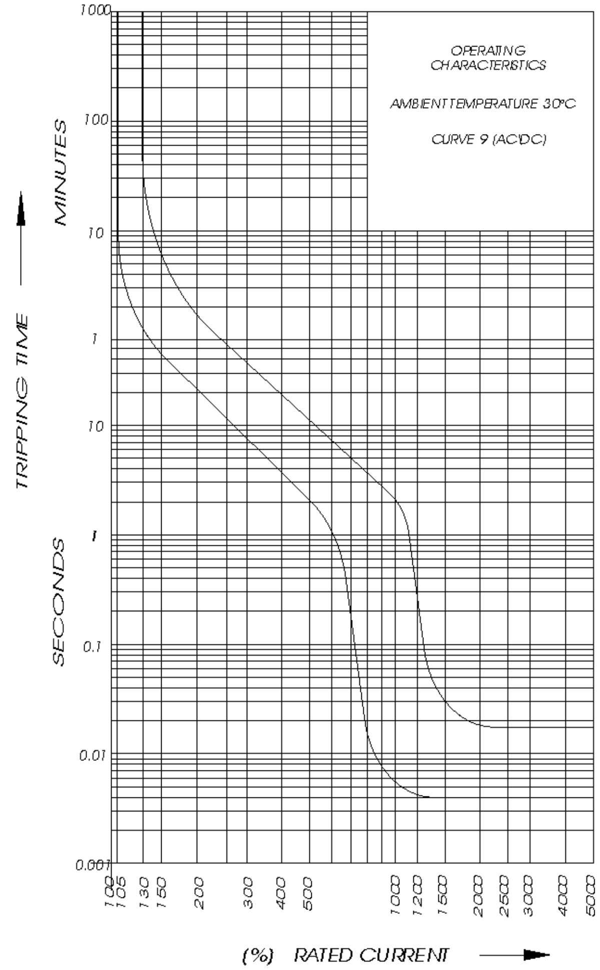

Figure 2.4 - Circuit Breaker Industries (CBI) Breaker Response Curve

One particular breaker, on the DC motor load line, was replaced by a fuse. Largely motivated by this experience, it was determined that as soon as reasonable, the original switchboard should be replaced by smaller, modular boards each crafted to handle certain amounts of current. Such modularity would have the added benefit of improving troubleshooting and repair turn-around time. As part of this process, it will be necessary to learn about the design and manufacture of high current PCBs. Kaha Sariashvili joined SuPER in January 2007 to design and test a board for the motor load, and suggest new designs for the switch board.

2.1.2 Status and Control Hardware

A/D conversion for data acquisition is accomplished by use of multiple National Instruments' (NI) USB-6009 Multifunction Data Acquisition (DAQ) devices. As indicated, they interface to a PC host via USB. All data that provides system status information to the PC for control comes in through these devices. The network of sensors, data acquisition devices, and PC software that manages the devices and data is collectively known as the SuPER status system. Figure 2.5 shows a simple block diagram of this system. The hardware of this system in its current state is partly the work of Gustavo Vasquez, as documented in his Spring 2006 senior project paper [8].

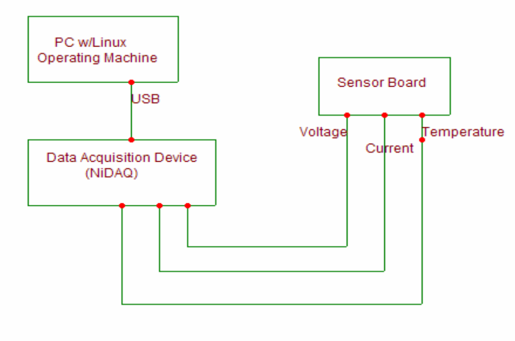

Figure 2.5 – Status System Interface Block Diagram [8]

There is a triple of key sensors (voltage, current, and temperature) at each of three essential locations in the system: the PV array, the DC-DC converter output, and the battery. In addition, the voltage and current are monitored at each load. Newly added in recent months is a pyranometer which outputs a voltage level corresponding to the level of insolation. Therefore the total number of status system inputs, M, is defined as: M = 10 + 2·L where L is the number of loads.

The current sensors used are the ZAP25 and AMP50 models manufactured by Amploc. Temperature data is provided by National Semiconductor's LM50 sensor.

Vasquez's efforts included sensor characterization and calibration, the construction of sensor circuit boards, and work on the status system data reading code. The sensor circuit boards are for converting the current and temperature sensor output voltages to proper levels for the A/D inputs. Also, the subsystem voltage levels are stepped down to required levels for the USB-6009 devices.

The pyranometer is manufactured by Apogee Instruments, Inc. and measures the insolation, which is the radiation between wavelengths of 300 and 1100nm incident to the Earth's surface [9]. The level of insolation outside the earth's atmosphere has been measured at 1370 watts per square meter (Wm^{-2}) [10]. The level incident to the earth's surface is less due to atmospheric attenuation and other factors, and the maximum terrestrial insolation observed by SuPER team members is just under $1100Wm^{-2}$. There is a reduction in incident insolation as the angle between the normal to the sun's rays and the line of propagation of rays to the point of measurement increases. Thus, equatorial regions receive greater insolation than other regions of the planet in general. The amount of reduction corresponds directly to the angle and this effect is expressed mathematically as Lambert's cosine law [9]; for this reason Apogee instructs that the pyranometer must be mounted parallel to the ground. The pyranometer is calibrated to output 1mV per $5Wm^{-2}$, or a maximum of 220mV at the full insolation level of $1100Wm^{-2}$. The value of $5Wm^{-2}$ in this ratio is determined by fabrication methods and materials, and is inscribed upon the device by the manufacturer. The manufacturer reports a temperature sensitivity of about .1% per degree C, for which we do not compensate at this time.

A circuit for amplifying the pyranometer output was constructed on a breadboard attached to the inner wall of the switch box, an effort supported by senior Slavic

Orzhakovsky. The circuit is diagrammed in Figure 2.6. We use an LM324 operational amplifier in a voltage reference configuration, powered with an LM340 voltage regulator which steps down the 12V system bus voltage to 5V. The measured resistor values are 9.87kΩ and 2.18kΩ for R_1 and R_2, respectively. This results in a gain A of 5.52.

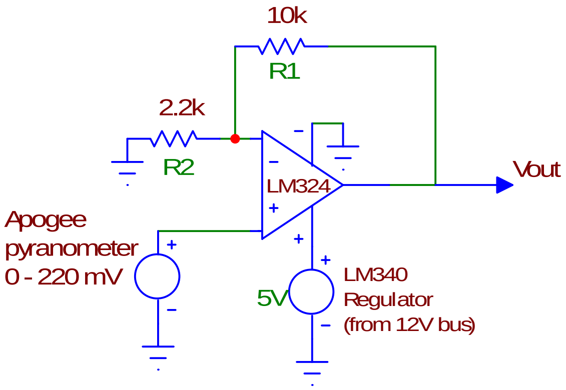

Figure 2.6 – Pyranometer Data Circuit

The output of the pyranometer amplifier is fed into analog input #7 on USB-6009 Dev1 and data recorded and stored by the computer software. In software, the amplifier gain A will be removed by division, and the resulting raw value in millivolts will be multiplied by 5000 to give insolation, G, in Wm^{-2}.

$$G = \frac{multiplier \cdot W/m^2/V \cdot V_{in}}{A} = \frac{5 \cdot 1000 \cdot V_{in}}{5.52}$$

All data produced by the status system is collected by the control system at a rate f_{ss}, defined as the status system sampling frequency. Its inverse is T_{ss}, which is currently set at two seconds.

There are N control system outputs where N is defined as N = 3 + L, where L is the number of loads. One of the outputs is the value of the duty cycle for the buck converter PWM signal. This value is usually spoken of as a percentage, with a minimum of 0 and a max of 100. In the PC software it is stored and manipulated as a floating point number, with values between 0 and 1. When transmitted serially to the PWM-producing microcontroller the value is first represented as an 8-bit unsigned binary number. The microcontroller code provides the proper mapping of the unsigned number to the desired duty cycle of the PWM output. The remainder of the outputs produce binary on/off values. These control the MOSFET switches that dictate the flow of current in the system. There is one switch each for the PV array and DC-DC converter, and one for each load circuit.

2.2 SuPER Load Characterization

2.2.1 Television

The television is the simplest of all loads considered. The unit which SuPER uses is a 12V DC black/white GPX portable TV/radio, equipped with a 5-inch screen. It draws a continuous current of between 600 - 700mA (8W). The television circuit is identified on the prototype as circuit #2.

2.2.2 Cooler

The Coleman 12V DC cooler was chosen to represent a typical low-power (60-70W) refrigeration device that might be used by families who have had no previous access to in-home refrigeration. The cooler load is identified as circuit #3. This particular model (5644) has a volume of 40 quarts, and uses a Peltier element to cool the interior down to about 40° F below ambient temperature. An empty cooler reaches this state in three hours. The power cable is equipped with a 7.5A fuse. For SuPER we wish to study methods of limiting the power needed in operating the cooler.

It was hoped that the cooler would require less power to maintain a minimum temperature than would be needed to reach it. Tests done with an empty cooler have shown this to be true. Figure 2.7 illustrates the decrease in power consumption over time for the cooler.

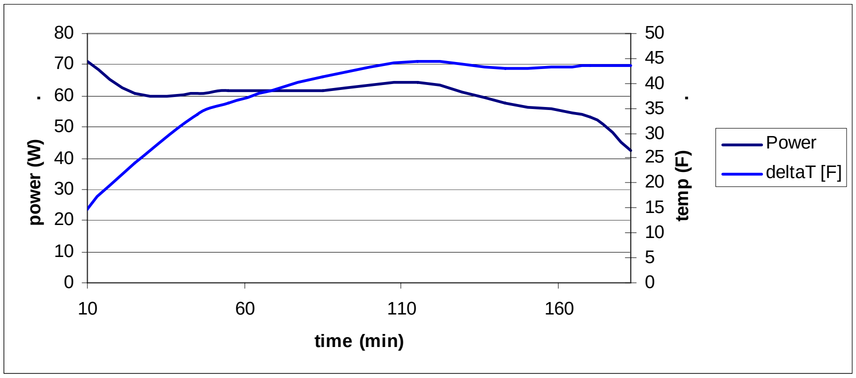

Figure 2.7 – Cooler Power Demand

However, an empty cooler being largely worthless, we choose to characterize it while under a "load" of eight quarts of water. It will likely be undesirable to invest the power necessary to bring eight quarts of water down to the minimum temperature. We will simulate and test towards maintaining the water between 20° and 30° F below ambient temperature. Note that due to the Peltier element, the difference in internal and ambient temperature is the key parameter [11]; the minimum interior temperature that can be achieved is highly dependent on the external temperature. If possible, it would be preferable to be able to control the temperature assigning some initial value, without sampling internal air or water temperature, and make control decisions purely based on the time needed for cooling.

Figure 2.8 shows the cooler air and water temperature over time as the cooler runs, as well as the difference between those and the ambient temperature. In this case, the ambient temperature experiences relatively small fluctuations.

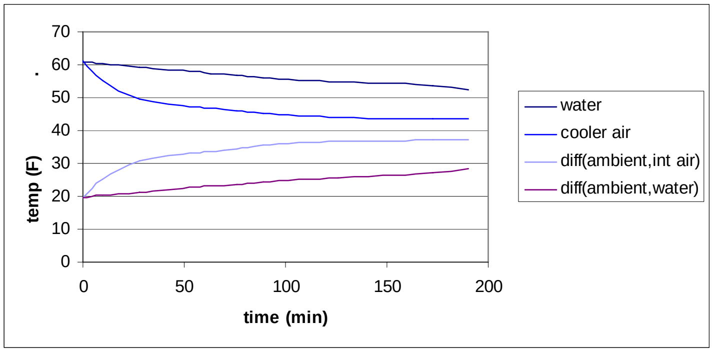

Figure 2.8 – Loaded Cooler Temperature Study

Most intriguing is the linearity with which the water temperature decreases. The downward rate of change of water temperature is approximately .05°F per minute. This linearity is also observed in a warming scenario; chilled water is placed inside the cooler, which contains air chilled to the same temperature. Equalization with ambient temperature (which, again, is fairly constant) has been calculated to be approximately .008°F per minute. The ratio of warming rate to cooling rate is .16. Thus, to maintain an average temperature, power theoretically need be delivered to the cooler for only 8.3 minutes of every hour.

This characterization is fine for very gradually changing external temperatures, but proves all but useless for rapidly changing temperatures. Figure 2.9 shows the results of a study done in which the cooler experiences three 60-minute power cycles, each nine minutes on and 51 minutes off.

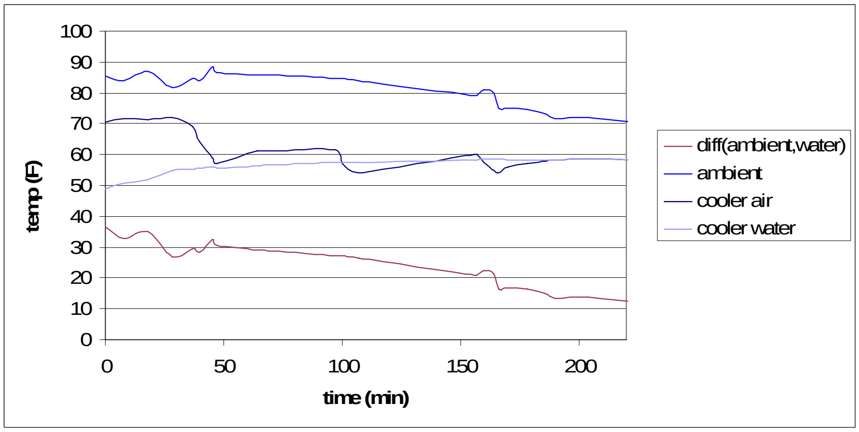

Figure 2.9 – Cooler 60-minute Cycle Temperature Study

The cooler on times can be identified by the corresponding drops in interior air temperature. One problem with this cycle period is the time taken for the interior air temperature to drop low enough to begin to cool the water, a sort of "setup time". It is likely more efficient to increase the cycle period so that setup times are a smaller ratio to total cooling time. A second study, with measurements plotted in Figure 2.10, extends the cycle period to 725 minutes. The cooling period occurs in the first 100 minutes.

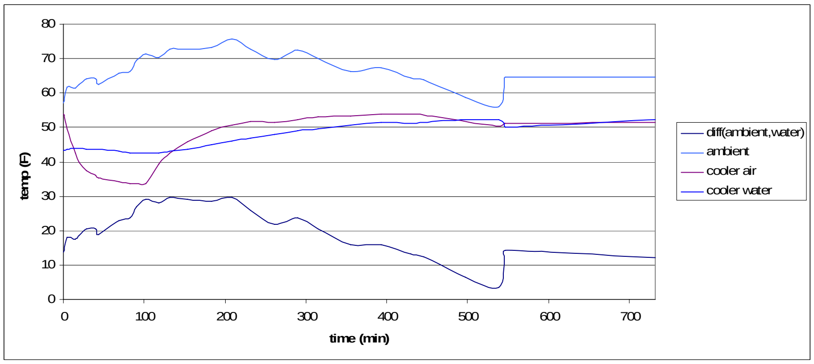

Figure 2.10 – Cooler 725-minute Cycle Temperature Study

At time 538 minutes, the cooler was brought indoors to provide a more constant external temperature, for reference and comparison purposes. The much more steady temperature difference rate of decline from that point onwards is clear. It can also be observed that the quickly increasing external temperature has a high impact on the rate of change of internal cooler air temperature when the cooler is unpowered. Maintaining some average difference between ambient and water temperature is difficult under variable conditions. If the cooler is to be run out of doors, it may be necessary to power the cooler much more often than desired. If that is accepted, perhaps some power savings can still be achieved while measuring only the ambient temperature and compensating by adjusting run times.

2.2.3 LED Lights

One of the primary functions of SuPER will be to provide a few hours of night-time lighting for the family home. The necessary energy will be drawn from the battery. It is expected that the control system will ensure that the day ends with the battery in a high SOC in anticipation of the energy requirements for lighting. It is essential however to find a type of lighting that provides high output, usually measured in lumens, at minimum energy use. To this end, SuPER will rely on the emerging LED lighting industry. The LEDs available today use about 3W of power and generate around 100 lumens each [12]. Unfortunately, operating at this wattage is inefficient. The SuPER prototype will instead operate the lights at a tad over 1W apiece. Four such LEDs will be allocated for use for the immediate future, requiring approximately 4.5W of power. The lights are designated as circuit #4.

2.2.4 Laptop

System status and control is run on a Dell Inspiron B120 laptop, chosen for its low cost (under $500). Specifications for the device declare it to be a 60W max system, drawing about 3A at about 20V. A converter is thus required for the 12V SuPER system bus to which the laptop will connect. A Lind Electronics Model # DE2035-966 converter was purchased from Dell; this converter will turn a 12-32V DC input into a 20V DC output at a maximum of 3.5A. It is equipped with a 15A fuse. Figure 2.11 shows the converter.

Figure 2.11 – Lind Electronics Model # DE2035-966 Converter

Information about the power and battery management system on Dell's laptops is proprietary, and therefore not available to the public. However, regular observation of the system in operation reveals some useful trends. The approximate battery SOC while charging from a wall outlet is recorded using the Windows XP battery meter, and displayed against time in Figure 2.12.

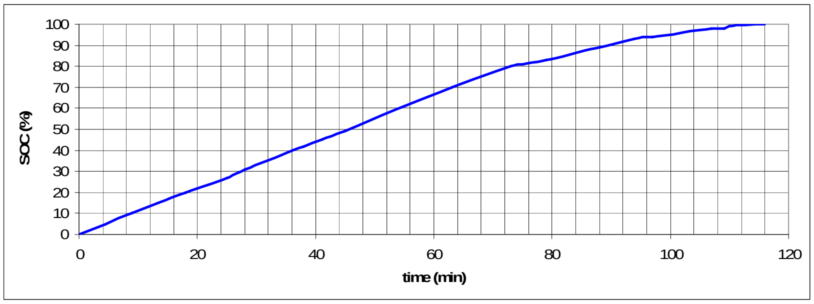

Figure 2.12 – Laptop Battery SOC Under AC Power

When powered by the SuPER cart, without its internal battery, the laptop draws approximately 2.5A (as considered from a system perspective and hence concomitant to a potential of 12V). With the laptop battery inserted, the behavior seems to change relative to the SOC of the battery. A depleted battery will perforce need to be charged, so the laptop will draw enough current to run the device and charge the battery in tandem. The laptop circuit will in this case draw two extra amps, for a total of 4 to 4.5A, which is closer to the specified maximum power requirement. With enough time passed to anticipate a fully charged internal battery, it is observed that the laptop has again reverted to a 2.5A current draw. Recorded data (see Figure 2.13) shows that there is a gradual drop-off in the current drawn by the laptop. Using the data from Figure 2.12, we can predict the time at which the battery reaches approximately 80% of charge capacity.

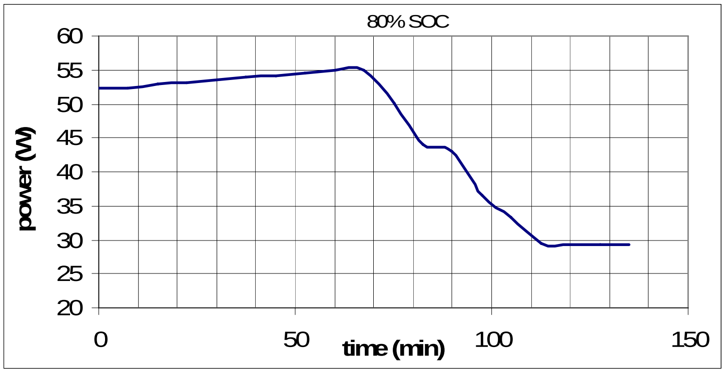

Figure 2.13 – Observed Laptop Power Needs Under Solar Power

This is fairly consistent with the known charging current requirements for lithium-ion batteries [13]. Lithium-ion batteries do not require a low-current trickle or float charge, and in fact may be damaged by such. Thus, the charge cutoff current is to be 0A. Figure 2.14 gives the shape of the expected lithium-ion battery charge current over time.

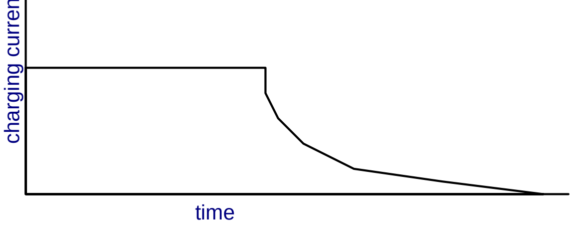

Figure 2.14 – Lithium-ion Battery Charging Current as a Function of Time

For the vast majority of the operation time of the system, the laptop will be a 30 – 35W load rather than a 54 – 60W load. This issue will be addressed in simulation by providing a variable load controlled by a laptop-specific function block. The mechanism is present for future use, but at this stage of development of the model the laptop battery is treated as always fully charged.

As the laptop is the intelligence of the entire SuPER prototype system, it is necessary that it be powered throughout the operating period of the system. It will thus be the last load to be disconnected from the system. We will not be relying on the laptop's internal lithium-ion battery for any sort of sustained operation of the status and control system at this time. It will of course provide a small amount of power-on current for the laptop when initiating system operation from a shut down state, and will only be depended upon for that purpose.

2.2.5 DC Motor

For the SuPER prototype, the team has equipped a ¼ horsepower, 12V permanent magnet DC motor which will be used to represent the water pump load. It is anticipated that this is the most demanding load to be powered by SuPER. Jennifer Cao's senior project report [14] records operational data for the motor, also echoed here in Figure 2.15.

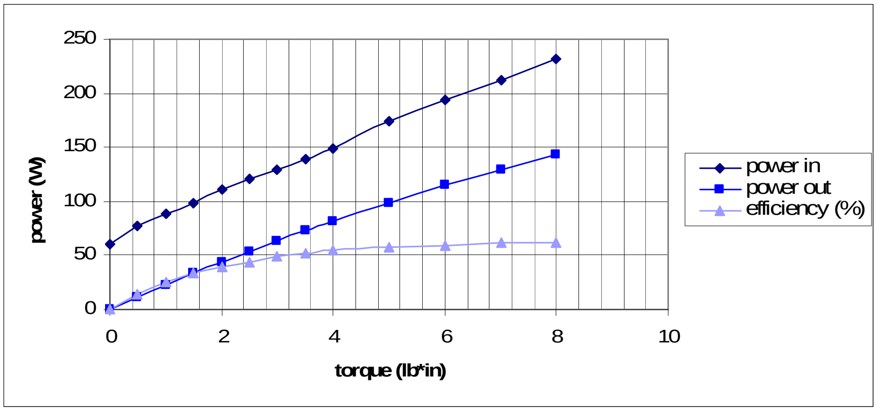

Figure 2.15 – Motor Load Power vs. Torque

For the SuPER prototype testing we will plan on operating the motor at a constant 8lb·in torque, which loads the motor to near the maximum rated power output. This is also a more efficient use of input power than operating at a lower torque. A dynamometer is used to load the motor.

On starting up the motor, there is a large amount of current drawn for a very short time period known as the inrush current, and is accompanied by a correspondingly large drop in battery voltage. Frequent repetitions of such current draw can have adverse effects on battery life over time if the battery charge is not maintained at a high level [15], and for this reason senior Joe Witts explores the advantages of including an ultracapacitor in the system for his senior project [16]. He reports that such a configuration provides negligible assistance in the case of infrequent motor activation. Cycled motor use, with a period on the order of a few minutes or less, can cut battery energy costs down significantly. A 58F ultracapacitor manufactured by Maxwell Technologies was purchased and will be introduced into the system. The motor load is circuit #6 on the prototype.

2.3 Battery Management

The SuPER prototype battery is a 12V valve-regulated lead-acid (VRLA) unit manufactured by East Penn (or Deka), rated at 98Ah for 20 hour discharge. The SOC of a lead-acid battery is a percentage representing the ratio of charge remaining to total battery charge. Its inverse is the depth of discharge (DOD). Determining the SOC for VRLA batteries while connected to a load has always been a difficult problem. The simplest, most typical way to make this determination in practice is to measure the open-circuit voltage (V_{oc}) of the battery, due to a nearly linear relationship between V_{oc} and SOC for lead-acid batteries [15]. This method provides a reasonably accurate assessment, however, it is unrealistic for many systems because a true V_{oc} can only be attained after all current flow in and out of the battery has been suspended for 24 hours [15]. This is not an option for the SuPER project. The general approach to this problem is to use frequent measurement techniques to estimate the SOC in software. Methods to this end are proposed by Vairamohan in [17], Duryea, Islam and Lawrence in [18], and Castaner and Silvestre in [19].

The SuPER team has chosen to use the model in [19] designed for PSpice but modified by team member Tyson Den Herder for Simulink as his senior project [20]. This model is divided into charge and discharge mode and provides a SOC estimation using the battery energy balance equation. Upon integration of the student-designed DC-DC converter, it is anticipated that this model will be ported to C code on the status and control laptop. In [21] Fasih provides some vindication of the model and methodology. Like SuPER, Fasih also made use of Hall effect current sensors and NI DAQ hardware for his measurements.

One shortcoming of the model in [19] is that it disregards the non-trivial impact of temperature on the battery state. Also, Castaner and Silvestre mention that the model realistically should be restricted to use for a SOC within a range of 30-80% of capacity, for which it will provide the best estimates. This provides a problem for SuPER, as we desire to always maintain as high a SOC as possible. The approach taken to this matter is detailed in chapter four.

Tal's thesis [2] Appendix B discusses the way battery charging is handled by the Outback MX60 converter. The device relies solely on PV and battery voltages for its calculations, as we will do with the Phase 1 system. Our goal will be to mimic the operation of the MX60 with our converter. The MX60 is a very expensive (and efficient) piece of hardware that was designed to handle much larger amounts of power than that associated with the SuPER prototype [22], [23]. It has three primary charge states: bulk, absorb, and float. While in the absorb stage, the MX60 gradually reduces current over time, and assuming plenty of available current will run approximately one hour. The battery documentation prescribes charging voltage levels for bulk and float stages (Figure 2.16), but makes no mention of an absorb stage.

Table 2.1 – Deka Battery Charge Voltage Guide [15]

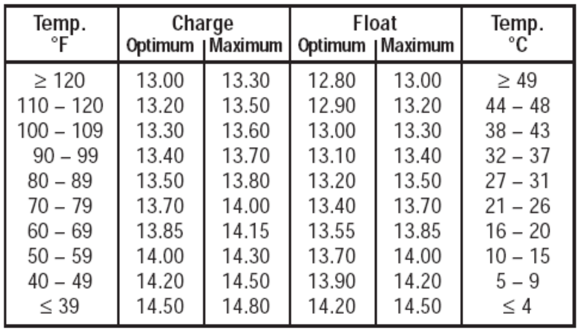

Temp. °F	Charge		Float		Temp. °C
	Optimum	Maximum	Optimum	Maximum	
≥ 120	13.00	13.30	12.80	13.00	≥ 49
110 – 120	13.20	13.50	12.90	13.20	44 – 48
100 – 109	13.30	13.60	13.00	13.30	38 – 43
90 – 99	13.40	13.70	13.10	13.40	32 – 37
80 – 89	13.50	13.80	13.20	13.50	27 – 31
70 – 79	13.70	14.00	13.40	13.70	21 – 26
60 – 69	13.85	14.15	13.55	13.85	16 – 20
50 – 59	14.00	14.30	13.70	14.00	10 – 15
40 – 49	14.20	14.50	13.90	14.20	5 – 9
≤ 39	14.50	14.80	14.20	14.50	≤ 4

The MX60 is programmed by the user with these voltage levels. The absorb stage is entered immediately after the bulk charge stage. Absorb and float stages are both employed only when the battery is in a high SOC. The primary concern for battery integrity is avoiding overcharging, which is the condition of supplying charging current when the battery is already at 100% SOC; hence the different charging stages recommended by the manufacturer [15]. For simplification of the SuPER status and control system, we will abandon the absorb stage and utilize only bulk and float charging. In discussions with Tal, he indicated that this was a reasonable simplification.

2.4 Phase 1

The closed-loop version of the system, in which all modules (besides the PV array, battery, and laptop hardware) are designed and created at Cal Poly, is called the Phase 1 system. Figure 2.17 is the Phase 1 block diagram. The SuPER team's goal was to complete this phase by March 2007. Critical to success in reaching Phase 1 is the implementation of a locally designed and built DC-DC buck converter specific to this application. The MPPT control would then be moved to the status and control PC. Two previous efforts at constructing a functional converter have already been made and did not succeed. Perhaps the SuPER team had underestimated the difficulty in implementing such a device for this high current application. Seniors Robert Casanova and Joe Shein began new efforts to develop the converter in fall of 2006. A second effort by seniors Thaddeus Guno, Koosh Shah and Kunal Shah using an alternate approach commenced in early 2007.

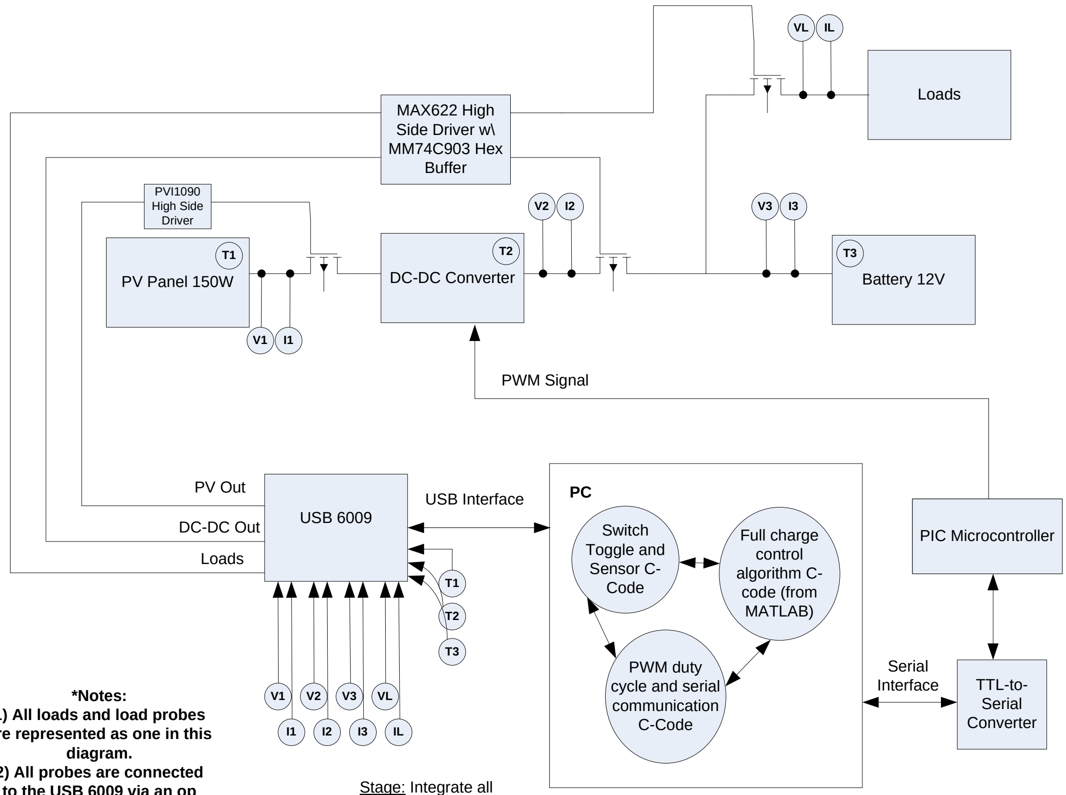

***Notes:**
1) All loads and load probes are represented as one in this diagram.
2) All probes are connected to the USB 6009 via an op amp gain circuit, omitted from this block diagram.
3) The combiner box, which doesn't appear in the block diagram, junctions all the power lines.

Stage: Integrate all individual system components to one unit on the cart

Figure 2.16 – Phase 1 Block Diagram [2]

The specifications given for the converter, derived from PV array and battery characteristics are:

Table 2.2 – DC-DC Converter Specifications [2]

Parameter	**Value**
Input voltage	wide range, 0 to 40V
Input current	4.75A max
Max power	150W, 80% efficiency target
Output voltage	11.5 – 14V
Output current	13A max
Switching frequency	500 kHz

See section 5.2.2 in [2] for more details on the specifications. Guno, Shah and Shah are designing a converter from the ground up [24], and their efforts will include layout of a high-current PCB. The 500 kHz PWM signal for this converter is sourced by a microcontroller, and some of the difficulties with this approach involve proper marriage of this signal to the MOSFET switch. Casanova and Shein are using an entirely different method [25]. SuPER has been provided with dual 75W buck converters as a donation from Linear Technology. These converters have a built-in PWM signal generation chip, which uses a resistive feedback line to maintain a constant 12V output. Some modifications were necessary to apply the device to SuPER, as the output cannot be constant due to the battery and loads. It was theorized that using different values of resistors on the feedback line would alter the response of the PWM generator chip and could be used to adjust the output voltage of the converter. Casanova and Shein proved this true, and a Maxim digital potentiometer (MAX5529) controlled by a two-wire serial interface is used to provide the changing resistance. Its 64-tap configuration will allow a 1.56% duty cycle resolution. Control of the potentiometer will be via the digital output ports on the USB-6009 device. Code written to communicate with the potentiometer (*potcomm.c*) has been tested successfully.

Perhaps the most useful of the proposed power sinks for SuPER, the LED lighting remained an untouched matter through the summer of 2006. LED lights are a continually evolving (and also pricey) technology; nevertheless, the Phase 1 system provisions their inclusion. The lights are the final of the five proposed loads the prototype will service in these experimental stages, and senior Joey Zukowski was tasked with equipping the devices for SuPER at highest energy efficiency.

An additional Phase 1 goal is the development of a user-independent control system which derives maximum use of each load while optimizing the life of the battery and preventing overcharging. Essential to the development of an optimal control system is a thorough understanding of system behaviors under a variety of conditions. It is therefore desirable to simulate the system and create a platform upon which control schemes can be developed, assessed, and adjusted as necessary. This ambition became increasingly important to the project as it became clear that the integration of the DC-DC converter would not be reached on schedule.

As mentioned previously, there was a misstep in plans for handling the system's current requirements on the switch board in the Phase 0 system. For a completely operational Phase 1 system, the issue must be solved. The team also determined to take advantage of these efforts to simultaneously increase the modularity of the system components; specifically, it would be valuable to physically separate PCBs of different purposes and current levels.

As summarized in Table 2.3, besides the work on the ultracapacitor, seven parallel efforts were made from October 2006 through March 2007 to reach the Phase 1 plateau. Some of the work by these Cal Poly seniors will require the inclusion of more digital control system outputs in the near future. Zukowski will develop a DC-DC converter to step down from the 12V bus voltage and deliver about 4.5W to four LEDs. The PWM will also be transmitted by the PC through the PIC and managed by voltage and current monitoring code, in order to achieve maximum efficiency with the LEDs. The PIC can provide two PWM outputs if need be. For immediate integration and testing, a purchased static-output buck converter will provide satisfactory output.

Table 2.3 – 2006-2007 SuPER Project Student Contributions

Project	Student Contributors
DC-DC converter development (device modification)	Robert Casanova Joe Shein
DC-DC converter development (computer-controlled)	Thaddeus Guno Koosh Shah Kunal Shah
High current PCB development, thermocouples	Shane Murphy* Juan Uribe*
Pyranometer integration	Slavic Orzhakovsky*
High current PCB development	Kaha Sariashvili
Simulation and software control	Tyler Sheffield
LED lights subsystem integration	Joey Zukowski
Ultracapacitor integration	Joseph Witts
** denotes independent study, as opposed to senior project contributors*	

Though his efforts are not associated with the Phase 1 objectives, Joe Witts will add an ultracapacitor between the battery and the loads and will need control signals for three switches to manage the charging and discharging of the capacitor. The main converter built by Casanova and Shein will require two digital outputs for a serial interface to a digital potentiometer.

Chapter 3: Prototype Software

3.1 Interface

The status and control system for the Phase 1 prototype is all managed on a Dell Inspiron B120 laptop computer. This machine is equipped with an Intel Celeron M 1.4 Ghz processor and 256 MB of DDR SDRAM. With a 40 GB hard drive, it is more than sufficient for SuPER's computing power and data storage needs.

The laptop executes all data acquisition and control code over a Red Hat Enterprise Linux WS 3 operating system. A few factors figure into the decision to use a Linux platform. First, one of the goals of the SuPER team is that all software for this project be developed as open-source and protected under a general public license (GPL). This will ensure that the work will be available for modifications and expansion, as well as learning purposes, for any who may want to take advantage. Second, Linux facilitates C development in general better than other platforms, and for this project the ease of access to system-level (kernel) function calls is of paramount importance. Thirdly, the project team at the time felt most comfortable developing in that environment due to significant previous experience with Linux.

NI provides a well-documented C application programming interface (API) to accompany their multifunction data acquisition (DAQ) devices [26]. The name of the package is NI-DAQmxBase 2.1. This API consists of C functions that provide direct access to and control over the devices. With these functions the user can, for example, define and start analog input sampling tasks and set digital output values. Appendix A, taken from [27], outlines the API.

The team encountered some trouble with Linux in regards to the integration and interface for the USB-6009 devices, and the lessons learned are mentioned in passing here.

The Targus 4-port hub uses USB 2.0 drivers, so it is essential that the latest version of the Linux kernel be installed on the host machine. Version 2.4.21-37 is not equipped with the proper drivers and therefore version 2.4.21-47 must be installed. Before halting execution of the interface software process, all tasks assigned to the devices must be stopped and cleared. Bypassing this step causes a glitch that will result in Linux losing the device identifiers; restoring functionality requires a device hard reset (disconnecting the devices from their USB power source/host). Unfortunately, the example code that NI ships with the devices, and upon which the SuPER code was built, seems to disregard this peculiarity. As the NI code is executed, the user receives instructions indicating that the process may be terminated by using the ‘ctrl-c’ command. This is the universal Unix process halt command. This command does not allow the process to exit gracefully, but ends its life by kernel override. As a result, the kernel somehow loses communication with the DAQ devices. The problem was remedied by adding code to alter the execution shell to return characters byte-by-byte from stdin with each key press. When a ‘q’ is pressed, the loop catches it and is able to stop and clear all active tasks before halting the process. See Table 3.1 for details on the USB-6009 device errors encountered by the SuPER team.

Table 3.1 – Known USB-6009 Errors

Error	Implication	Action Required
Shell message: Device identifier invalid	Linux has lost track of the DAQ devices	Hard reset of DAQ devices
Shell message: Physical channel specified does not exist on this device	No known cause	Hard reset of DAQ devices
Shell message: Onboard device memory overflow	Host processes have taken away system resources from the USB-to-PC data transfer (or less likely, the sample rate is too high)	Close all other executables, and do not run anything besides status and control program
Sensor readings are bogus, such as large negative temperature values	The device identifiers have been mixed up	Hard reset of DAQ devices

3.2 Functional Overview

All initialization and parameterization of NI-DAQ tasks is handled in function main of the SuPER code, which is found in *contAcquireNChan.c*. The code enters an unterminated while loop that repeatedly reads the values out of the storage buffers recorded by the USB-6009, and displays them onscreen. Thousands of values are loaded by the USB-6009 into the buffers, and the NUM_TO_OUTPUT definition fixes the number of samples that are extracted (NUM_TO_OUTPUT must be less than or equal to the integer bufferSize). The extracted values are all averaged to formulate the display quantity.

The loop is executed at the system sample rate f_{ss}. At the beginning of each loop cycle, the buffers are checked to see if the write time has been reached (as defined by TIME_FACTOR, in minutes). The values must be periodically written to the hard drive so as not to be lost. The written values consist of all samples extracted prior to averaging. Thus, the written files contain NUM_TO_OUTPUT / T_{ss} samples per sensor for each second of run time and the total number of samples per sensor in the file is TIME_FACTOR * 60 * NUM_TO_OUTPUT / T_{ss}.

Hard drive accesses are expensive operations, and it is important not to delay the time-sensitive loop commands so as to avoid the risk of device memory overflow. Therefore, main is forked so that a child process may take care of the file I/O and the parent can return promptly to data reading. Sensor data is written to the hard drive in comma separated value (.csv) files. The files are named with date and time included, e.g. "SuPER Wed Jan 10 10:44:30 2007.csv" and stored in a brother folder to the source code entitled *data*. To ease the manipulation of these large amounts of data, an Excel macro has been created that consolidates the file into one minute samples. See Appendix B for an introduction to this macro.

After each data set is observed and averages calculated a call is made to *pnopal.c* for running the control algorithm. *pnopal.c* contains the MPPT algorithm and sends the new duty cycle value to the PIC by calling *commpic.c*. *commpic.c* is the code that provides serial communication from the PC to the UART on the PIC. Figure 3.1 is a software flow diagram that summarizes all the simultaneous processes in execution when the status and control software are running.

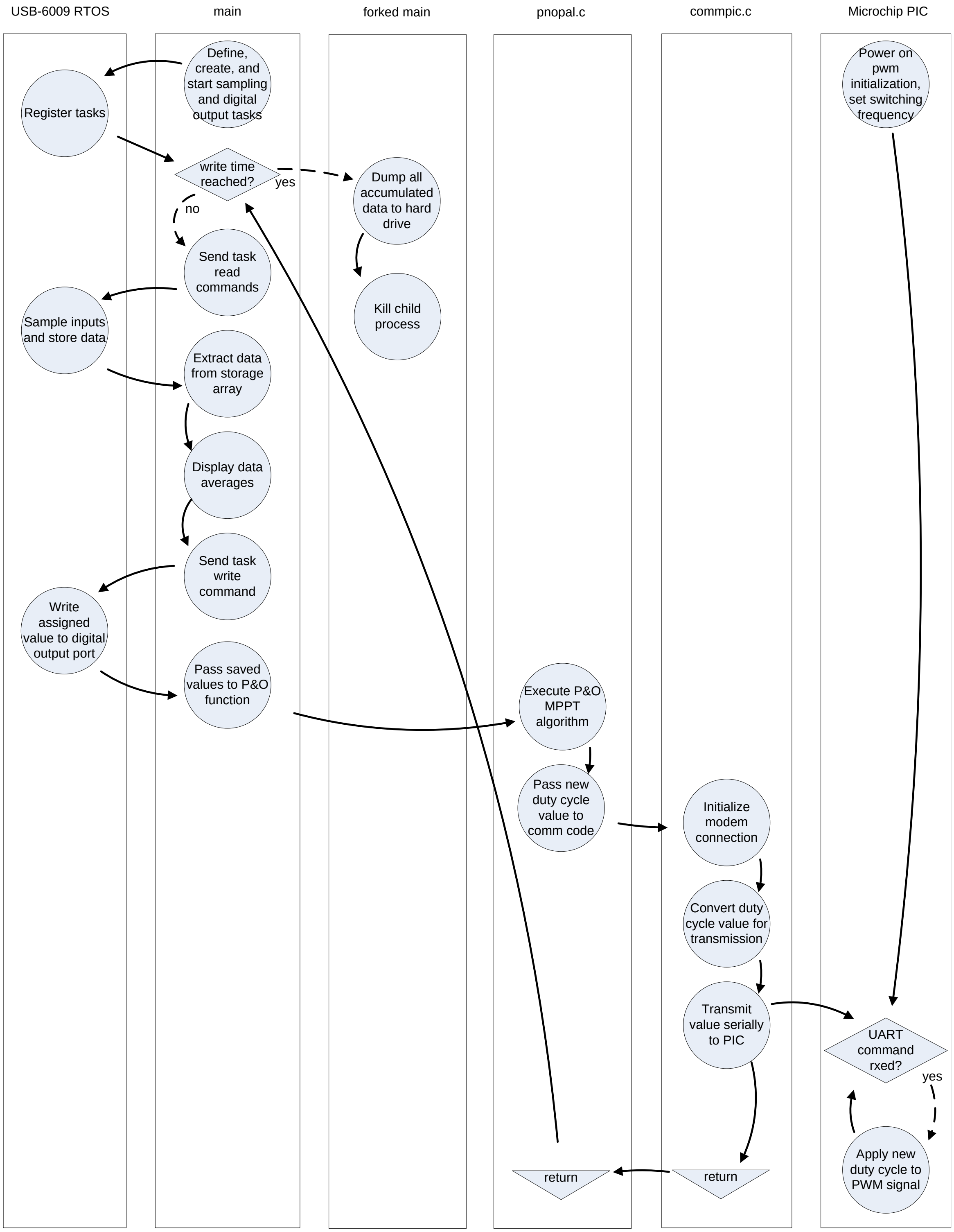
USB-6009 RTOS
main
forked main
pnopal.c
commpic.c
Microchip PIC
Define, create, and start sampling and digital output tasks
Register tasks
write time reached?
yes
no
Dump all accumulated data to hard drive
Kill child process
Send task read commands
Sample inputs and store data
Extract data from storage array
Display data averages
Send task write command
Write assigned value to digital output port
Pass saved values to P&O function
Execute P&O MPPT algorithm
Pass new duty cycle value to comm code
Initialize modem connection
Convert duty cycle value for transmission
Transmit value serially to PIC
return
return
Power on pwm initialization, set switching frequency
UART command rxed?
yes
Apply new duty cycle to PWM signal

Figure 3.1 – SuPER Software Flow Diagram

3.3 Control

The diagram of Figure 3.2 details the locations of all Phase 0/1 control inputs and outputs.

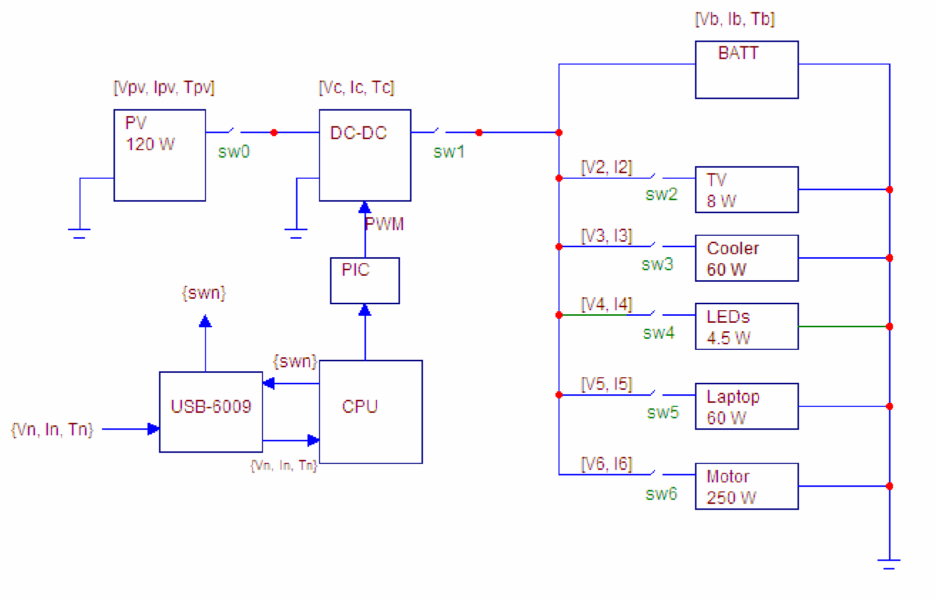

Figure 3.2 - SuPER Status and Control Interface Diagram

MPPT is accomplished with the simple and commonly-used perturb and observe (P&O) algorithm. The algorithm is presented in detail in Aki Oi's thesis [28] section 3.5.1, but briefly outlined here. The purpose of the algorithm is to maintain an impedance seen by the PV array that will cause the array to output power at peak capability. This is done by adjusting (perturbing) the DC-DC converter duty cycle at periodic intervals and monitoring the resulting array power output, through current and voltage measurements. A negative change in the power output will cause a reverse in the direction of the perturbations; a positive difference has the opposite effect. Figure 3.3 shows the location of the maximum power point on the I,V curve of the BP150SX solar panel at peak output.

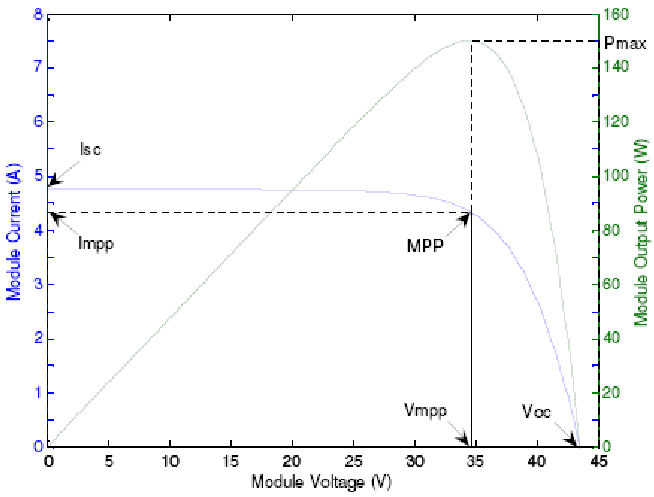

Figure 3.3 – BP150SX I,V and Power Curves [28]

The status system sample period T_{SS} (currently set at two seconds) puts a maximum rate on the control algorithm execution. Note that this is entirely different from the NI DAQ device A/D sample rate, which is much higher. Observation of the performance of the MX60 converter shows rapid response times under quickly changing conditions. The SuPER team attempts to mimic this capability, and will also run the control algorithm at the maximum rate. It is anticipated that the host machine will have adequate time to run the few necessary floating point multiplications and divisions between samples and that computational time overruns will not be an issue. The DC-DC converter transient response, discussed in more detail presently, will not be an issue at this rate.

The prototype currently makes use of a PIC 18F4320 microcontroller which can provide a 500 kHz PWM output. This is an upgrade from the 50 kHz signal provided by the original Phase 0 hardware, a PIC 16F877A. The PIC code is written in assembly language and compiled with the MPLAB development kit provided free of charge by

Microchip. Programming is achieved with the K128 USB 40-pin programmer from DIY Electronic Kits (http://www.kitsrus.com/pic.html).

The laptop is not equipped with a serial port, so the connection to the PIC is accomplished via a USB to serial conversion cable. The cable manufacturer is unknown, but the conversion chip is a product of Prolific Technology Inc; the model number is PL2303. Use of this cable in Linux requires driver installation and configuration.

Figure 3.4 - USB-Serial Cable with PL2303 Chip

It was necessary to develop a simple communication protocol for all serial transmissions between the PC and the PIC. The communication is largely one way, as the PC issues all commands and accompanying values. The microcontroller sends no data to the PC, but does respond to successfully received commands and values by returning an exclamation point character (!). UART serial communication is byte-oriented, and for ease of implementation all commands and values are eight bits in length or less. An explanation of the communication protocol can be found in Appendix C.

The battery model code from the Simulink model has been ported to the laptop, in the form of a function called *batt_voltage* in *contAcquireNChan.c*. It currently monitors battery current flow to estimate the actual battery SOC in real-time. Output is written with frequency f_{ss} to *Super_Output.csv*.

The prototype control software is largely incomplete as some of the hardware goals for the end of March 2007 were not attained. The only form of control currently implemented in the prototype software is the MPPT algorithm; even so the generated output is actually of no practical use without a DC-DC converter. The prime resource for developing and testing control algorithms, then, is currently the Simulink simulation.

Chapter 4: MATLAB Simulink Model

4.1 Model Overview

The new Simulink system model builds upon the foundation established by Tyson Den Herder in his senior project [20], but attempts to reach far beyond its limits and uses a different development approach. The primary difference between Den Herder's efforts and what is to be accomplished in this thesis is a matter of construction, detail, and scale. In the conclusion of his report, Den Herder makes some observations and recommendations on improving the model, all of which are addressed in the model presented here. Figure 4.1 is a view of the entire SuPER Simulink Model.

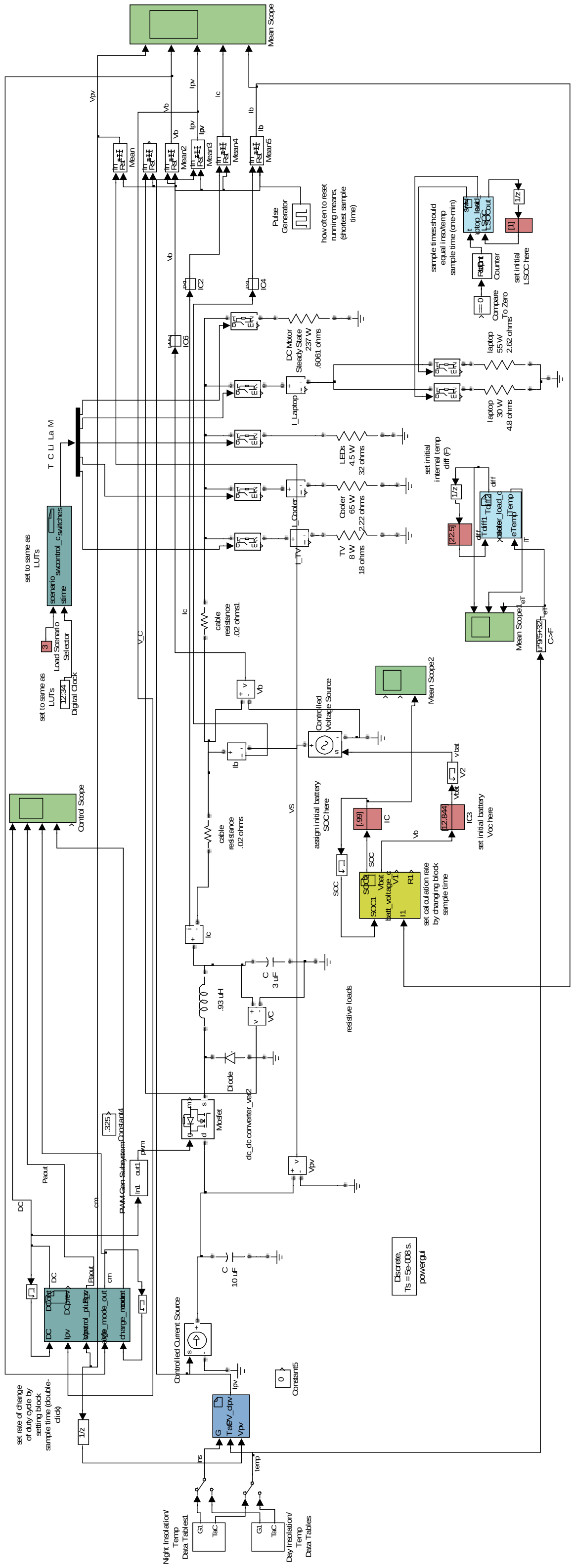
Mean Scope
Vpv
Vb
Ipv
Ic
Ib
Mean
Mean2
Mean3
Mean4
Mean5
Pulse Generator
how often to reset running means (shortest sample time)
IC2
IC4
IC6
sample times should equal insol/temp sample time (one-min)
Counter
Compare To Zero
set initial LSOC here
1/z
laptop 55 W 2.62 ohms
laptop 30 W 4.8 ohms
DC Motor Steady State 237 W .6061 ohms
I_Laptop
LEDs 4.5 W 32 ohms
Cooler 65 W 2.22 ohms
TV 8 W 18 ohms
I_Cooler
I_TV
set initial internal temp diff (F)
diff
Mean Scope1
C->F
T C Li La M
set to same as LUTs
Load Scenario Selector
Digital Clock
cable resistance .02 ohms1
V_C
Controlled Voltage Source
Mean Scope2
cable resistance .02 ohms
assign initial battery SOC here
SOC
IC
IC3
set initial battery Voc here
V2
vbat
VS
set calculation rate by changing block sample time
Control Scope
C 3 uF
.93 uH
VC
resistive loads
Diode
Mosfet
dc_dc converter_ver2
PWM Gen Subsystem
Constant4
.325
pwm
Discrete, Ts = 5e-008 s. powergui
C 10 uF
Controlled Current Source
Constant5
DC
Pavail
Pout
cm
set rate of change of duty cycle by setting block sample time (double-click)
ins
temp
Night Insolation/ Temp Data Tables1
Day Insolation/ Temp Data Tables

Figure 4.1 – SuPER Simulink Model

Each component of the model will be presented in detail. For orientation assistance, a generalized map of the key components and connections in the model is offered in Figure 4.2. Red lines represent electrical connections, while blue lines are purely inter-block signal lines.

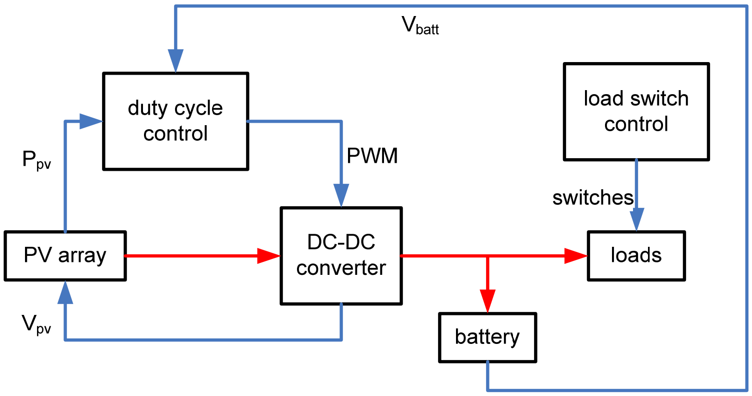

Figure 4.2 - Simulink Model Map

In Simulink there are three methods of expressing the functionality of operational subsystems, or modules: component blocks, mathematical function building blocks, or MATLAB code (also C/C++,etc). Den Herder used the function block construction method for the battery, control and converter subsystems. To assist the Simulink model in better reflecting its real-life counterpart, the converter was recreated by Dr. Harris using the component blocks available in the SimPowerSystems package. In a nutshell, this means building the converter out of capacitors and inductors, etc., rather than representing it with a collection of mathematical function blocks. For modularity, reproducibility, and optimization purposes the battery and control modules were remade as S-function blocks of code.

4.1.1 Design Approach

Figure 4.3 shows the typical configuration of a simple buck converter.

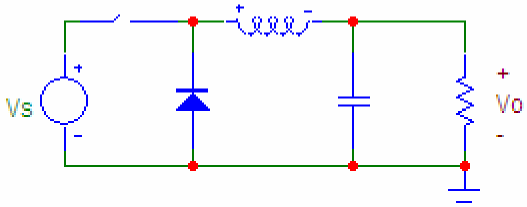

Figure 4.3 - Simple Buck Converter

The DC-DC converter MOSFET switch is driven by a 500 kHz PWM signal, a rate defined by the capabilities of the PIC 18F4320. The energy storage components (an inductor and capacitor) are the key converter parameters chosen based on the desired response of the converter. The inductor value (L) is .93mH, calculated using the equation for the desired maximum converter output current, from [29]:

$$I_{\max} = V_0\left[\frac{1}{R} + \frac{(1-D)}{2 \cdot L \cdot f_{sw}}\right]$$

D is the duty cycle as a fraction of value one, f_{sw} is the switching frequency, and R the load resistance. The capacitor size (C) is determined by the desired ripple on the output voltage (ΔV_o), and found for this model with the help of some experimentation to be 3μF. This is the relationship, from [29]:

$$\Delta V_o = \frac{D \cdot \overline{V_o}}{R \cdot C \cdot f_{sw}}$$

In a typical buck converter configuration with resistive loads, the potential produced by the front-end source, V_s, is “bucked” to a desired average output V_o by altering the switching duty cycle accordingly. The relationship is

$$\overline{V_O} = DV_S$$

For this application, the output voltage is anchored to values near 12V, on a range of about 10 – 14V, by the battery. Duty cycle adjustments will instead reflect on the converter input voltage, which is the voltage V_{pv} at the PV array terminals. This voltage, in conjunction with the temperature and available insolation, determines the amount of current output by the array. Figure 4.4a shows the voltage that is seen by the array as a function of the duty cycle in the Simulink model of SuPER. The relationship is not linear. This plot shows curves for three different insolation levels, all at a constant load of 68 W, a typical load scenario. Alongside is an example of how the array I,V curves may look for these different levels.

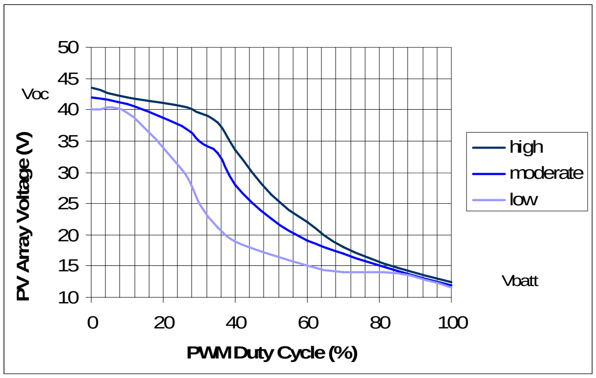

Figure 4.4 a) – PV Array Voltage Response for Varying Insolation Levels (68W Load)

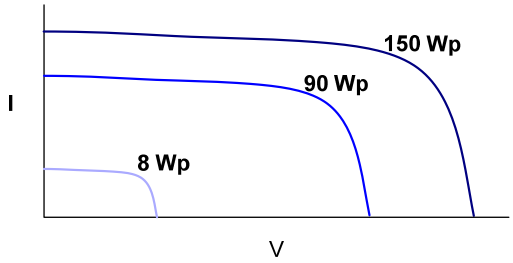

Figure 4.4 b) – Example of Corresponding I,V Curves

Unexpectedly, interfacing the current source to the DC-DC converter in Simulink presented a non-trivial problem. The software recognizes that with the MOSFET switch closed, the circuit topology presents an inductor in series with a current source. This is an illegal configuration as the inductor current would not be independent. It is therefore necessary to include some circuit element in parallel with the current source. Various options were explored, including resistors and controlled voltage sources, but a capacitor actually provides the optimum system behavior. This is because the capacitor offers stability in maintaining the converter input voltage, which is used to calculate the PV array current. If the capacitor is too large, the response time will be too slow and the voltage level will never rise; if too small, it does not provide the needed impact and the voltage will fluctuate far too much. A good value for the capacitor was found by experimentation to be on the order of microfarads, in this case 10μF. Thus, the Simulink model includes an extra 10μF capacitor on the converter input due to the manner in which the PV array is modeled for simulation purposes.

Voltages and currents plotted with Simulink scopes oscillate at the switching frequency. The output voltage ripple is intended to be minimized by careful attention to the capacitor chosen for the converter; to smooth the output to a greater extent and allow the developer to see some semblance of average DC values, Simulink offers two options, neither of which are ideal for this use. One option is the weighted moving average block. Weights need to be assigned to each sample, and the number of weights determines the "window" size. This makes it impractical for windows of thousands of samples, and has proven difficult to use in practice. The chosen method is a reset enabled running mean block, whose reset period is a confirmed hazard in simulation. The optimal period seems to be twice the fastest S-function block sample period. The running mean blocks must be reset on the falling edge of the reset signal, so that any downsampling does not catch the block output early in the new mean processing, as the oscillations will result in unsettled sampled values.

4.1.2 Function Blocks

Desiring a modular simulation model, we made prolific use of MATLAB's S-functions. These are created as blocks in the Simulink model editor, but completely defined by MATLAB code in associated m-files. There are a variety of S-function types, but the original system design was done with these particular blocks; they are known as Level II M-file S-functions. The function that is to be implemented can be written in MATLAB language just as would be done for execution or function call from the MATLAB command line. However, creating an S-function requires wrapper code around that function code. Ports must be enumerated and identified for each input and output of the block. The function code is placed in a separate section for determination of the outputs. One drawback of these S-functions is their lack of internal memory. In other words, the function is executed top-to-bottom continually with no memory of previous states.

Efforts to speed up the simulation process led to a new approach to the S-functions. The software is greatly hampered by the need to call the M interpreter each time M-file S-functions are invoked. By writing the code in C instead, and pre-compiling it before runtime, the simulation time can be greatly reduced. This variety of function block is known as a C-MEX S-function. Running one simulation on a 1.4 GHz machine for the M code blocks required 22 hours. The same simulation on the same machine with the new C code blocks runs in under two hours.

Insolation and temperature data are located in lookup tables (LUTs) as described in Den Herder's senior project [20]. We will continue to use Oi's model for the PV array, as defined in his thesis paper [28]. Figure 4.5 is a diagram of this model, which was implemented in MATLAB code for simulation.

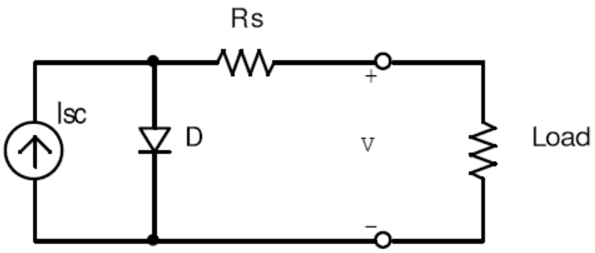

Figure 4.5 - PV Array Model [28]

The insolation, temperature, and array voltage are fed to the PV array S-function, which simply provides a wrapper for Oi's BP150SX solar panel m-file. For the new C code blocks, the solar panel code was translated to C. The PV block outputs the current produced by the array, which is built electrically as a controlled current source driven by the S-function output. Figure 4.6 shows the PV S-function block.

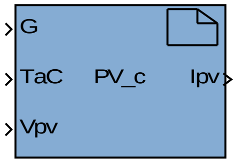

Port	Identity
G	insolation (Wm^{-2})
TaC	Temperature (ºC)
Vpv	PV voltage (V)
Ipv	PV current (A)

Figure 4.6 - PV S-function Block

Note that although the array is rated by the manufacturer at 150W peak, in practice the SuPER team has observed a maximum output of only 122W at peak insolation. An adjusting coefficient has been added to the array code to reflect this.

The control algorithm with P&O code for the MPPT is contained in an S-function block titled Control (Figure 4.7). The Control block also requires initialization and knowledge of a couple of values, as MPPT operation is dependent on the system's behavior under previous outputs. Thus, the current duty cycle (parameter DC, which is not to be confused with direct current voltage/current) and charge mode (cm) are assigned initial conditions and fed back through Memory blocks. The charge mode parameter has two possible values, 1 or 2, which correspond to bulk and float charge stages respectively. The stage is adjusted according to the battery voltage, V_b.

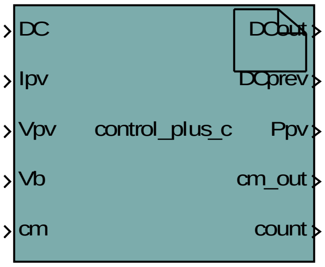

Port	Identity
DC	duty cycle initialization (%)
Ipv	PV current (A)
Vpv	PV voltage (V)
Vb	battery voltage (V)
cm	charge mode initialization (1,2)
DCout	new duty cycle (%)
DCprev	old duty cycle (%, for debug)
Ppv	PV power (W, for debug)
cm_out	old charge mode (1,2)
count	mode restriction (0,1, for debug)

Figure 4.7 - Control S-function Block

In the switch control S-function block, load operation decisions are made. For this early version of the control system, a table is created that holds the on and off times for each of the five loads. The code then uses the system time to flip the load enabling switches on and off. There is a scenario selection input that lets the model user identify which load time table to use. This block is shown in Figure 4.8.

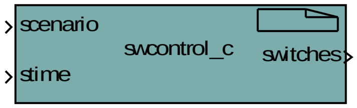

Port	Identity
scenario	load scenario identifier (0:13)
stime	system time (sim minutes)
switches[0:4]	load control output (0,1)

Figure 4.8 - Switch Control S-function Block

Of special relevance to SuPER is the battery model in use. Den Herder's simulation uses the PSpice model from [19], adapted to Simulink. Table 4.1 identifies the parameters associated with this model.

Table 4.1 – Battery Model Parameters

Parameter (Units)	**Significance**	**Type**
k (%)	battery efficiency	constant
SD (h^{-1})	self-discharge rate	constant
n_s	number of series 2V cells	constant
SOC_1 (%)	initial SOC percentage	constant
SOC_m (Wh)	battery capacity	variable
SOC (Wh)	estimated remaining energy	variable
β (%)	SOC / SOCm	variable
I_1 (A)	battery current	variable

The model uses these parameters to predict the battery internal resistance (R_1) and terminal voltage (V_{bat}) at time t. Den Herder uses a 12V, 66Ah @ 20 hours (792Wh) capacity battery. SuPER's Deka 8G31 model is rated at 97.6Ah @ 20 hours (1171Wh) so the model must be updated accordingly. The charge/discharge efficiency value, k, is not made available by the battery manufacturer, so following one of the examples given in [19] and echoing Den Herder's choice, a conservative value of 0.8 will be applied. This coefficient is a multiplier of the battery current in the model SOC equation, so adjusting it will impact the rate of change of the SOC in both charge and discharge states, for charge associated with the current flow. This parameter was not used in making adjustments to the battery model because of the need to account for differences in charge and discharge behavior.

It is also necessary to adjust the self-discharge rate, which is provided by the manufacturer. According to the specifications (Figure 4.9) the battery will linearly lose

50% capacity over a 16 month period, assuming it is sitting at typical room temperature (20ºC).

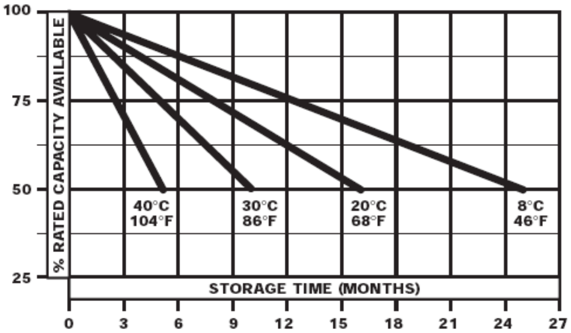

Figure 4.9 – Deka VRLA Battery Self-discharge Chart [15]

This information yields a discharge constant of 4.34e-5 h^{-1} (.5/11520 hours).

Another critical battery parameter is SOCm, the total energy capacity in Wh. This value is a function of the current draw, and follows a somewhat logarithmic curve. Seven current/capacity data points are available in [30] only for the absorbed glass mat (AGM) version of SuPER's gel 8G31DT. For the gel variety, we know only that the capacity is 97.6Wh @ 4.88A, which is slightly less than the AGM battery. In consequence we must estimate what the gel battery curve may look like, starting from the one known point. Figure 4.10 shows the provided AGM curve and the estimated gel curve.

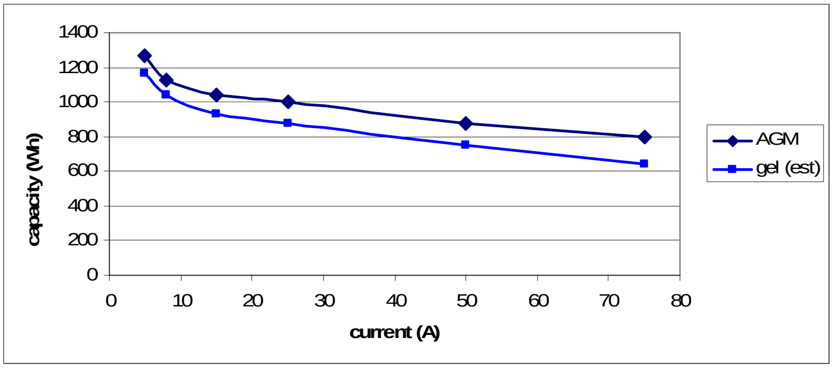

Figure 4.10 - Current vs. Capacity for AGM and Gel Batteries

It was necessary to make adjustments by adding code to estimate the capacity SOC_m for different battery currents (I_b in Simulink, equivalent to the model's I_1). For currents in excess of 2A, we will use the logarithmic function derived from curve-matching in Excel to make the estimate:

$$SOC_m = -179.68 \cdot \ln(I_b) + 1435.2$$

For currents less than 2A, a value of 1325Wh is used. The battery S-function is shown below in Figure 4.11.

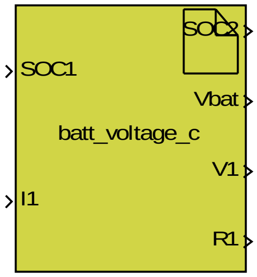

Port	Identity
I1	battery current (A, same as I_b)
SOC1	SOC initialization (%)
SOC2	new SOC (%)
Vbat	battery voltage (V)
V1	internal voltage (V, for debug)
R1	internal resistance (Ω, for debug)

Figure 4.11 - Battery S-function Block

The battery model requires an initial SOC, and some sort of state memory to properly update the battery condition throughout the simulation runtime. The SOC is fed back into the battery model input through memory blocks so that previous outputs will be held on the signal line.

The creation of the battery S-function is followed by the adaptation of the model to the performance characteristics of the battery in use. At our disposal is the battery charge and discharge test data acquired under operational conditions by Tal and published in [2]. It is essential to note that the authors in [19] state that the battery model presented is only accurate for a SOC range of 30-80%. Model adjustments can then be made experimentally in an attempt to match the data recorded while the battery SOC was in this range. Castaner and Silvestre provide an example of adjusting parameters to fit a commercial battery, but unfortunately do not explain their methodology. Doing our best to follow their lead, the same parameters will be altered.

Exactness in the battery model is not our chief concern, but some precision for the 80-100% charge range would be beneficial as we hope to consistently maintain a high SOC on the battery. The team adopted what is the perhaps the only reasonable approach to this issue, which is to use Tal's data to make adjustments to the model in use for an alternate high SOC case. The most difficult decision to make is how to model the battery in the tricky 80-90% charge range. This is just above the model's effectiveness range, and according to Tal still within the bulk charge mode breadth for the MX60 (which extends to approximately a 90% charge).

The model is divided into four SOC states: 80% and below, 80-90%, 90-100%, and 100% or higher. This final state, largely to be avoided, simply provides a high terminal voltage so that the control algorithm is able to prevent overcharging. Shown here are the resulting equations for the 90-100% SOC range, within which the SuPER team would like to operate the battery most of the time. As in [19], multipliers are added to the R_1 and SOC equations, and the V_1 (open circuit voltage) equation is slightly adjusted.

Discharge Mode

$$V_1 = (1.95 + .18 \cdot \beta) \cdot n_s$$

$$R_1 = (.19 + \frac{.1037}{\beta - .14}) \cdot \frac{n_s}{SOC_m} \cdot 50$$

Charge Mode

$$V_1 = (2 + .148 \cdot \beta) \cdot n_s$$

$$R_1 = (.758 + \frac{.1309}{1.06 - \beta}) \cdot \frac{n_s}{SOC_m} \cdot 15$$

SOC

$$SOC = SOC_2 + \frac{1}{SOC_m} \cdot ((k \cdot V_1 \cdot I_1 - SD \cdot SOC_2 \cdot SOC_m) \cdot t) \cdot 0.625$$

See the C code in Appendix D for the equations pertaining to the remainder of the states.

Den Herder's implementation includes a for loop with which the model integrates over time to calculate the new battery SOC, and the loop was used to dictate a step size and rate of SOC updates. This allows the user to start with a given SOC and find the resulting SOC after any period of time with the battery under some known constant current flow. The for loop was removed for the new simulation, as the steady state current will be changing at a known rate equivalent to the highest frequency clocking found in the model (most likely the control block). Since the current may, and likely will, change with each duty cycle adjustment we desire to update the battery conditions at the same frequency. We can thus fix the integration time window to be the sample time of the highest frequency clock in the model, which will necessarily be the same sample time of the battery function.

The work done in characterizing the various loads under operating conditions allows the implementation of some of the loads as S-function blocks, containing code that reflects actual power demands and responses. In the case of the cooler load, given the operating parameters described in chapter two, the load will be represented only by a resistor in this first generation of the model. However, a function block (Figure 4.12) was constructed to perform the temperature adjustments constantly occurring inside the cooler; currently it is only effective for slowly changing external temperatures.

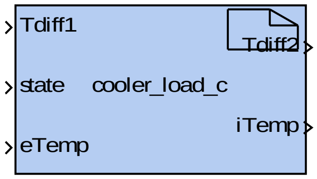

Port	Identity
Tdiff1	initial temp difference (ºF)
state	on/off condition (0,1)
eTemp	external temperature (ºF)
Tdiff2	new temp difference (ºF)
iTemp	internal temp (ºF)

Figure 4.12 - Cooler S-function Block

The laptop load S-function block will take as input the estimated initial SOC of the laptop lithium-ion battery, as well as the time under power and use a mathematical model derived from actual performance data to decide on the resistance of the load.

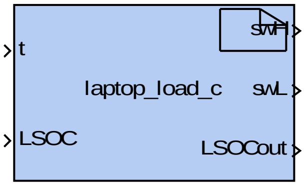

Port	Identity
t	charge time (m)
LSOC	battery SOC initialization (%)
swH	switch for high power load (0,1)
swL	switch for low power load (0,1)
LSOCout	new battery SOC (%)

Figure 4.13 - Laptop S-function Block

The charge time port, t, is driven by a running counter which is reset upon activation of the laptop load switch. The laptop's battery management system charges the battery at a nearly constant rate until it appears to begin to limit charge at around 80% capacity. See chapter two for the laptop characterization.

The available Simulink packages at our disposal do not include a variable resistor. Thus only two laptop current draw options are provided for the simulation: low draw for a full battery, and high draw for a non-full battery. In order to approximate the total power needed by the load over time, the switch from high current draw to low should take place when the battery SOC is estimated at 90%. At this stage of development, the laptop is always implemented as the lesser of these two loads as it is always considered to have a fully charged battery each morning.

4.1.3 DC Motor Subsystem

The design of the DC motor load proved to be an interesting problem. Initially it was planned that Oi's Simulink motor model should be copied, despite the fact that he was modeling a different motor than SuPER's. However, Witts was able to obtain more information about the motor parameters from the equipment manufacturer and in conjunction with experimental data was able to develop an accurate model for our motor in PSpice [16]. This model was then ported to Simulink, shown here as Figure 4.14.

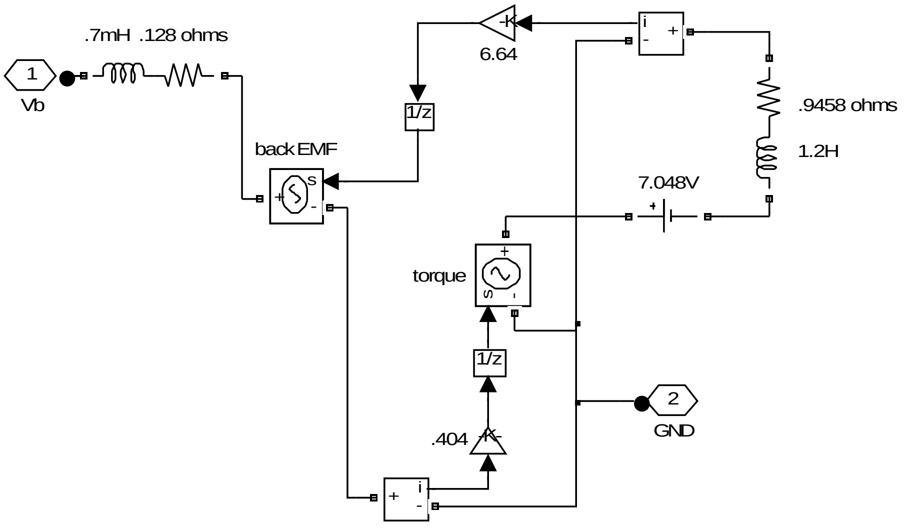

Figure 4.14 - Simulink Motor Subsystem

This configuration uses current-controlled voltage sources to represent back EMF and the torque of the load. The torque is a constant 8 lb·in. Algebraic loops made unit delays necessary for the current measurements driving the voltage sources (see section 4.2 for more on algebraic loops). The simulation results are given as Figure 4.15. These results are achieved using an 11.75V constant source as a power source for the motor.

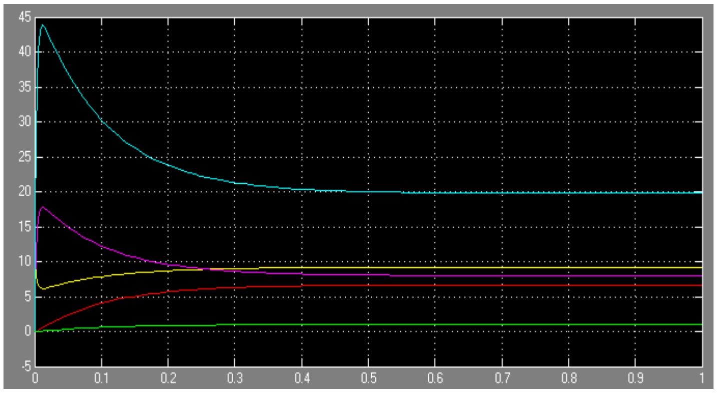

Color	Identity
cyan	battery current (A)
magenta	torque (lb·in)
yellow	battery voltage (V)
red	back EMF voltage (V)
green	speed (krpm)

Figure 4.15 - Motor Transient in Simulink (time in s)

The motor has near to a 500 ms real-time transient response. Because of our need to speed up the simulation process, system changes are made at much faster rates. We therefore cannot get accurate results using the motor model as shown in the simulation of the model if we desire reasonable simulation times. For broader scope system simulations, we will replace the motor subsystem with a .6Ω resistor representing a 237W load. For an analysis of the transient response while the motor is in-system, we can adjust the sample times for the other subsystems in the model to allow the motor transient to proceed uninterrupted as it would on the prototype. Figure 4.16 shows the simulated transient response.

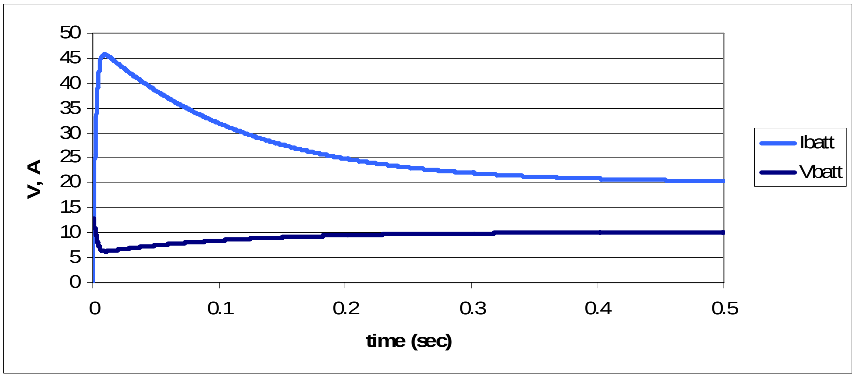

Figure 4.16 - Motor Simulink Model Load Transient

Witts will install a 58F ultracapacitor that will serve to protect the battery from deep current draw. A version of the Simulink model with the ultracapacitor included was created and simulated. As can be seen in the simulation results (Figure 4.17), the battery current does not jump up to 40A, but gradually increases; it nears the 20A steady state level in about 30 seconds.

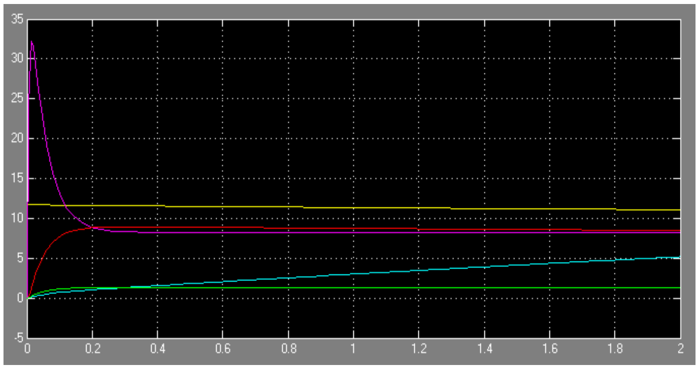

Color	Identity
cyan	battery current (A)
magenta	torque (lb·in)
yellow	battery voltage (V)
red	back EMF voltage (V)
green	speed (krpm)

Figure 4.17 - Motor Model Simulation with Parallel 58F Capacitor (time in s)

4.2 Principles of Timing and Sampling

One of the key issues confronting the creation of a system simulation is the handling of the various rates of system elements such as the MOSFET 500 kHz switching frequency, the rate of environmental data sampling, the control system operation rate, and the battery and load data update rate. We would have preferred to run the simulation in continuous mode with a variable-step solver for the sake of accuracy. However, such simulations have proven to be far too computationally intensive and time consuming to be a realistic option. A discretized simulation is necessary, but fraught with its own perils.

Choosing a solver can be a frustrating issue. Simulink has a variety of available continuous and discrete time solvers, and it is not always clear which one will serve the model's purpose best. Appendix E contains information on choosing solvers distilled from MATLAB's user guide [31]. For SuPER, it was realized that no continuous states were necessary in the model and the fixed-step discrete solver was chosen; however, the model has matured enough now that many of the fixed-step solvers appear to be viable.

Variable-step solvers are not an option, as they do not tolerate the presence of the running mean blocks and choke on "mixed sample time" errors.

There is a delicate tradeoff between the system sample time and the resolution for the duty cycle. For power efficiency, we would clearly like the resolution to be as small as possible, but that comes at a cost. The duty cycle resolution is the product of the switching frequency (f_{sw}) and discretized simulation sample time (T_s).

$$DC_{step} = f_{sw} \cdot T_s$$

Increasing the sample rate comes with the cost of increased simulation time and memory requirements. However, long sample times can make the duty cycle resolution too coarse to allow a realistic simulation, as the converter will be forced to sacrifice large amounts of power. Figure 4.18 illustrates the effect that a discretized simulation has on the ability to differentiate between duty cycles. The black line is the PWM signal as it would be output from a signal generation block. The blue markers are samples spaced at 1/Ts, and connecting the markers would represent the PWM signal as it is passed to the MOSFET. In this case, DCstep (the duty cycle resolution) has been found to be 5%; a duty cycle of 5% in (a) holds no surprises. In (b) we see that increasing the duty cycle to 9% will in practice be the same as a 5% value. We must increase to 10% as (c) shows in order to the see the change. Similarly, in the opposite direction, (d) a 1% duty cycle is the same as 5%.

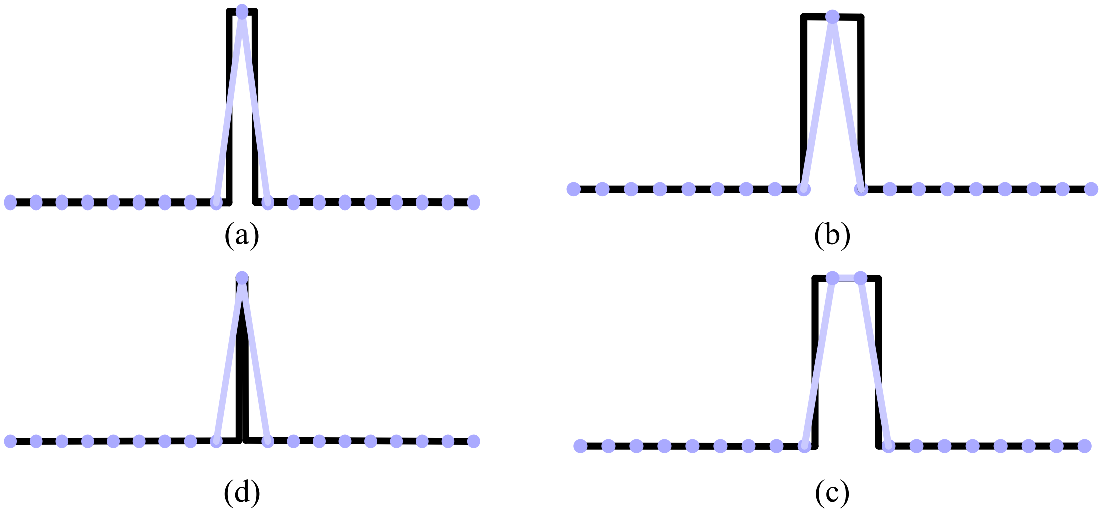

Figure 4.18 – PWM Signal Sampling: a) 5% Duty Cycle b) 9% c) 10% d) 1%

In order to prevent the solver from infinitely looping on the m-file S-function math operations (which occurs because of the feedback inherent in the model) we were forced to "clock" the function by only allowing access to the mathematics on the edge(s) of a pulse signal. The outputs are then only evaluated once per instance at a rate we specify. For the C-MEX S-functions, a function execution sample time can be defined. This is accomplished by a setting on the Initialization tab on the S-function dialog boxes. The block sample mode is set to Discrete, and the sample time directive defines the "clock" period. The PV array S-function cannot be "clocked" or sampled at a rate less than the discrete system sample time, unlike other S-functions, because the array would be unable to respond properly to the system changes which occur at high rates due to the converter switching frequency.

Insolation and temperature data for a 24 hour day are stored in blocks of 1,440 samples, supplying one sample per minute. Since the MOSFET switches at 500 kHz, the discretized simulation sample rate must be at or above the Nyquist rate of 1 MHz. Running a simulation on such a scale yields a terrific number of data points, unwieldy for the PCs we are using. We must therefore fool the system by decreasing the insolation and temperature sample times artificially. For example, we'll take one day's worth of data, but tell the simulation that it is one second's worth instead. As long as the transient response of the converter (Figure 4.19) is not interfered with, the simulation time can be greatly reduced. Such a change will also affect real-time values in hours used in the battery SOC and load current draw calculations, so an adjusting time coefficient is included in those functions.

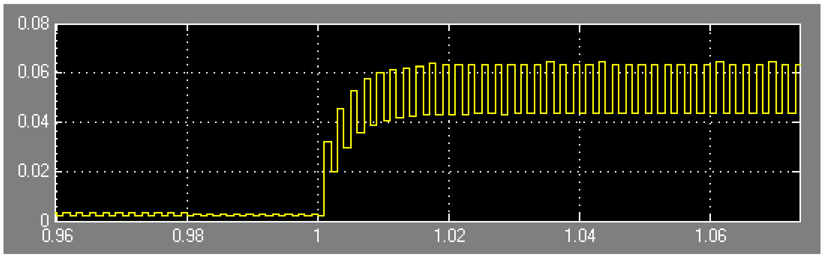

Figure 4.19 - Discretized Converter Transient Response (time in ms)

Here we are interested in the time scale; the values shown on the x-axis are milliseconds. Thus, the transient response is shown to be well below 50 μs. The short response allows the simulation time to be decreased significantly. For the simulations in chapter five of this paper, one minute in real time is equivalent to one millisecond in simulated time. The discrete system sample time and switching frequency factor into the speed at which the simulation can be calculated. The chosen values result in a simulation that takes approximately one second in real time for each millisecond in simulation time. At this rate, a simulation of 24 hours of data can be completed in about 24 minutes.

The governing factor for the control system update rate is the rate at which we wish to change the PWM signal duty cycle. For the prototype, we would like to change the duty cycle as fast as the system sample time, T_{ss}, which will be the maximum rate. In

Simulink, since we want a real-time minute to be as short in length as possible we must severely cut back the number of duty cycle adjustments per minute so as to maintain the 24 minute completion time for the simulation. Table 4.2 holds the final values for the key sample times in the model:

Table 4.2 – Final Model Sample Times

Entity	**Time (s)**
System	5e-8
Insolation/Temperature Data	1e-3
Control Block (duty cycle)	2e-4
Switch Control Block	1e-3
Battery	2e-4
Laptop	1e-3
Cooler	1e-3
PV array	5e-8
Running Means	1e-4

The system requires a PWM signal generation block that can dynamically modify the duty cycle of the signal. There is no such block in the Simulink library so it was necessary to create one; the new subsystem is shown in Figure 4.20. The duty cycle value is used to alter the phase and amplitude of a sinusoidal signal oscillating at the switching rate. The resulting sample is fed as input to a threshold-based switch, which produces either a zero or a step and alternates to form a square wave output. This dynamically adjustable PWM signal generation subsystem is confirmed to operate equivalently to Simulink’s PWM block.

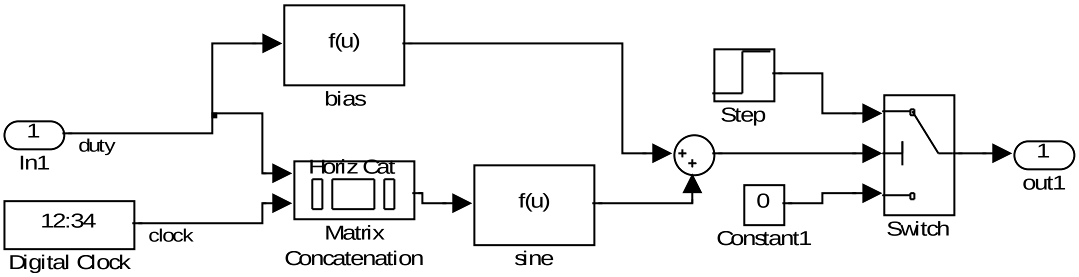

Figure 4.20 - Dynamically Adjustable PWM Signal Generation Unit

The sine function block output expression is

$$2 \cdot \frac{\pi}{T_{sw}} \cdot t - 2 \cdot \pi \cdot (D \cdot 50 - .25)$$

where T_{sw} is the inverse of the switching frequency (in this case $2e^{-6}$), D is the duty cycle value and t the simulation time. The bias function block output expression is

$$-\sin(\pi \cdot (.5 - D))$$

One of the problems with the earlier versions of the system which included the PV array, converter, and simple battery were algebraic loop errors. These result from the necessity of feeding back certain values into the function blocks. There were particular difficulties with the PV block; the source voltage V_s (V_{pv}) which is determined in part by the PV array current output, also serves as an input to the PV block for use in calculating the current. Simulink's help files declare: "An *algebraic loop* generally occurs when an input port with direct feedthrough is driven by the output of the same block, either directly, or by a feedback path through other blocks with direct feedthrough" [31]. In many cases, Simulink has the ability to successfully navigate through the algebraic loops. However, one particularly insidious problem was a simulation-halting loop calculation error that would occur partway through a run and could not be foreseen. The only known solution is to eliminate all loops completely with a work-around: adding a delay on the feedback path (in the form of a 1/z Unit Delay block). The amount of delay is one sample of the system sample time. This much delay will not adversely affect the S-function block output calculations, as it is negligible in comparison to the clocking rate of any blocks.

Once the simulation was able to proceed without encountering loop errors, it was found that the simulation strained system memory resources. The amount of data needing to be recorded overwhelmed our machines. We attempted to alleviate the problem with severe downsampling, and eliminated all signal probing at less important locations. Simulink's downsampling blocks, available in the Signal Processing toolkit, allow the user to specify the downsampling ratio and offset. Later a more elegant solution was discovered in the scope blocks themselves. The scopes can be instructed to perform decimation on their inputs (see Appendix F). We must see at least one sample for each event that alters the "steady state" of the system, since we are not interested in tracking the details of the transient system response. Thus, the maximum amount of decimation is determined by the block with the least sample time (L_s) according to the following

$$Dec \le \frac{\text{shortest block period}}{\text{system sample time}} = \frac{L_s}{T_s}$$

Of course, decimating at the maximum and running a simulation for less than T_s in duration will result in zero data points. Steps for accessing detailed simulation characteristics via Simulink's coverage reporting capability are found in Appendix G.

At this stage, all major barriers to running a successful simulation have been overcome. Though there are several minor tweaks and improvements that can be made, simulation results have provided encouraging validation for the usefulness of this model.

Chapter 5: Observations and Model Authentication

5.1 Exploratory Simulations

We wish to operate all loads as much as possible, however SuPER's ability to do so is dependent upon the power that can be harvested from the sun. There are certain hours of the day considered peak, at which much more solar energy is available. These are the prime hours for operating the more demanding loads.

The season has not enabled us to acquire insolation and temperature data for a typical summer San Luis Obispo day, so for investigative simulations we use data from a sunny May day in Golden, Colorado (Figure 5.1); this is the same data used by Den Herder in his simulations [20]. Time 0 represents 6:00 AM, while time 1439 corresponds to 5:59 AM the following day. All daytime plots in this chapter likewise use a minute-based time scale, starting at 6:00 AM.

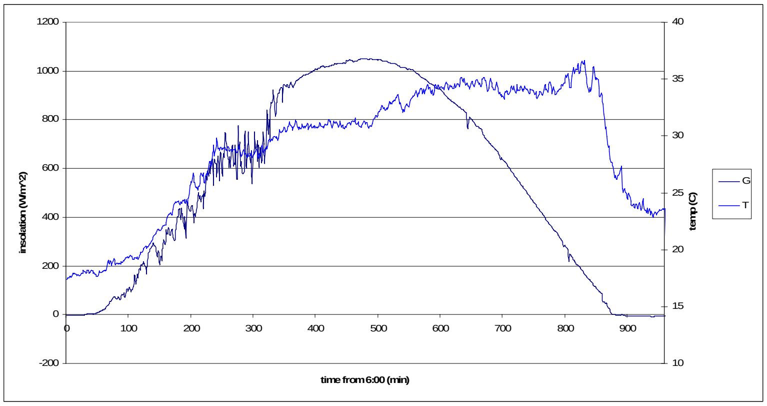

Figure 5.1 - Golden, Colorado Insolation and Temperature

By way of comparison, Figure 5.2 shows insolation and temperature data for a partly cloudy March day in San Luis Obispo, typical of the majority of the month. Almost 10 daylight hours are represented here. Peak insolation for these March days appears to be around 420 minutes (13:00).

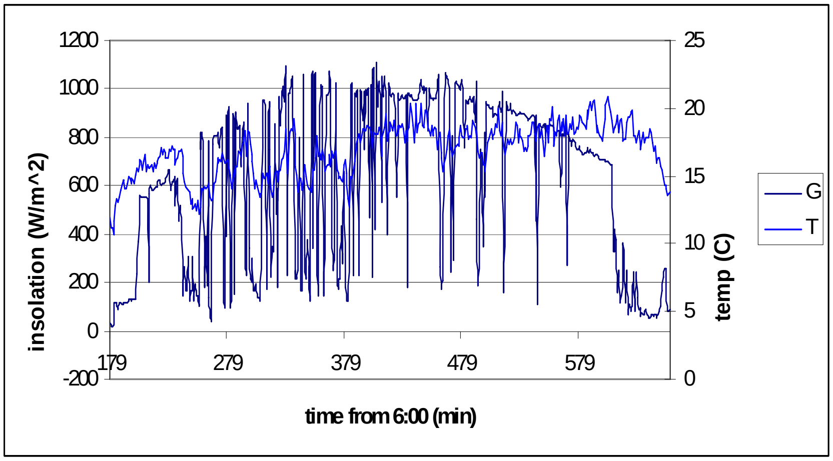

Figure 5.2 – San Luis Obispo Insolation and Temperature

For the control system it is essential to be able to distinguish between periods of differing levels of insolation, and this is done primarily by monitoring the power produced by the array. Despite the fact that for development purposes the insolation measurements are available to the control system, it is not anticipated that an installed system will be accessorized with a pyranometer. Thus, control decisions will not actually be made based on measured solar insolation. Of paramount importance to the project is extending the life of the battery, so the two key factors in load operation will be battery SOC and power produced by the array (P_{pv}), which is directly affected by the actual insolation level.

Note that the prototype uses a laptop for all status and control operations, so this will be taken into consideration for all simulations. Thus, it is presumed that the laptop will be drawing power during all daylight hours during which a load might be operating, and any nighttime hours during which it is planned to run other loads (particularly lights).

We will operate under the assumption that the laptop's on/off state is controlled intelligently by an external entity, such as a human user.

There are many questions the simulation can answer for us, which we can then verify through prototype operation. For example, it will be important to know how long the LED lights can be run in the evening, given the stipulation that the battery should be able to be recharged to full capacity the following day. The Figure 5.3 plot shows the result of four simulations, each representing some number of hours after sunset for which the LED lights are powered. Insolation is shown for perspective. Note that time 0 in this case does not represent 6:00 AM, but represents one hour before sunset instead.

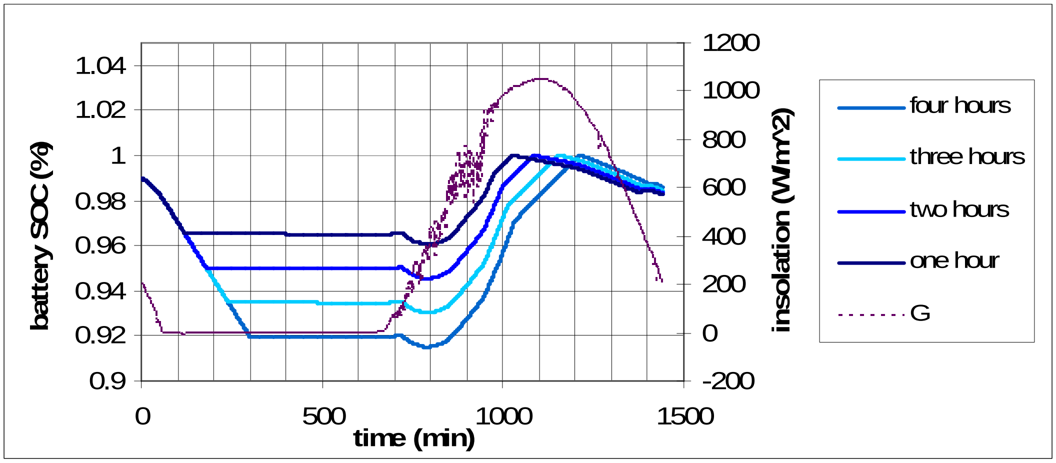

Figure 5.3 – Nighttime LED Operation Simulation

As the lights are powered for a longer period of time, the next morning must begin with less available battery charge and more time is required for the battery to reach full capacity. The slight dip in the early morning SOC shows an hour or so passes before the sun alone provides enough energy to power the laptop. Also, the overcharging protection code, dependent upon the battery voltage, is the cause of the slight fall in SOC at the end of the day.

As the heaviest load, the motor will only be operated in daylight and for a short time. For the sake of argument, let us run the motor for one continuous hour per day. The Simulink model can help determine when the most favorable hour for motor operation falls during the day. It may be tempting to assume that running the motor at peak insolation (approximately 13:30 to 14:30) is the best option. However, it may prove wiser to operate the motor in the morning hours and take advantage of the afternoon sun to recharge the battery. Figure 5.4 is a plot displaying the battery SOC over the course of the day for different hours of motor operation.

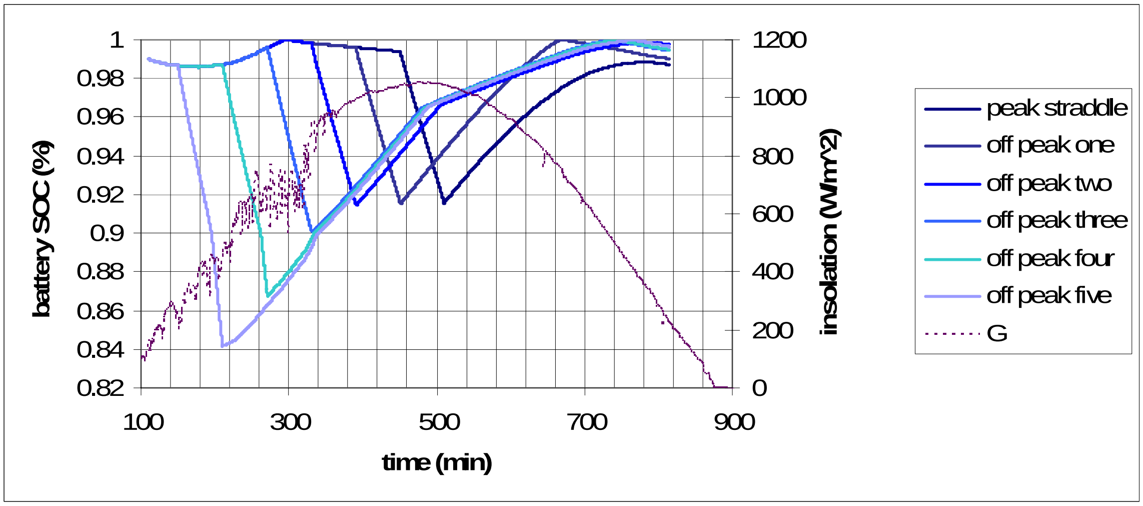

Figure 5.4 – Motor Operation Simulation

We wish to drain the battery as little as possible, and still be able to recharge it fully before the day is through. According to these simulation results, the hypothesis may prove correct. Operating the motor at around one to two hours before peak insolation should only deplete the battery to a little below 92%, and enough sunlight time will remain for a full recharge. The inconsistency in the recharging curves of these various scenarios can be attributed to the difficulty in modeling the battery while in the current-limiting float charge stage.

5.2 Result Validation

The next step towards proving the value of the simulation is to compare actual prototype system measurements to simulated versions of equivalent operating conditions. The preliminary exploratory simulations have assisted in defining what kinds of tests should be run. This first case illustrates the three-hour nighttime lighting situation in which the laptop alone is run for one hour with the lights joining for the final two. The data of Figure 5.5 is the battery voltage and current taken from the status system measurements.

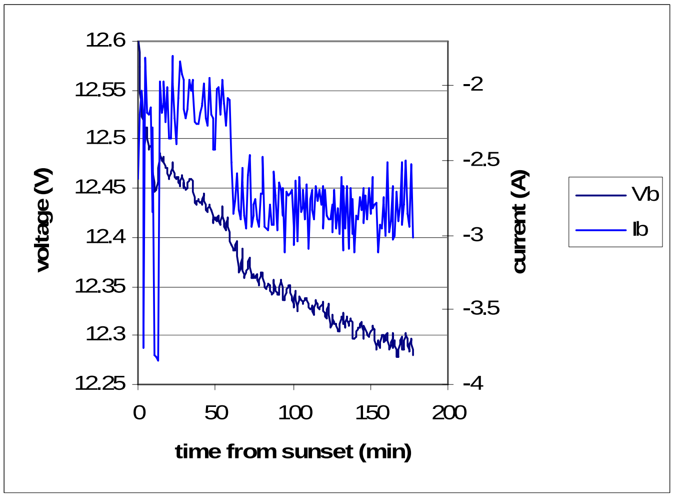

Figure 5.5 – LED Light Two-Hour Measurements

The early aberrations are likely due to the laptop battery taking on a small amount of charge. Figure 5.6 shows the results of simulating the same scenario.

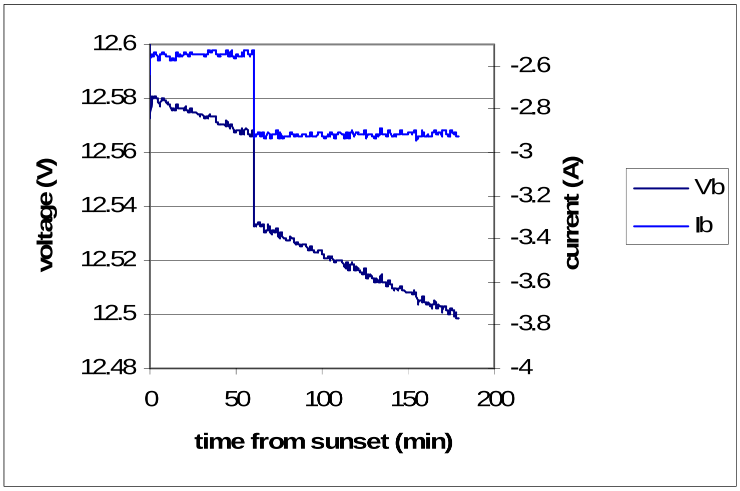

Figure 5.6 – LED Lights Two-Hour Simulation

The simulation predicts higher battery current draw and voltage. The lights draw a relatively small current, and a heavier load will be a more interesting case to examine. The prototype was placed under test with the motor load on March 19th, 2007 – a fairly sunny day with intermittent cloud cover. Shown in Figure 5.7 is the insolation and temperature data for about five of the daylight hours.

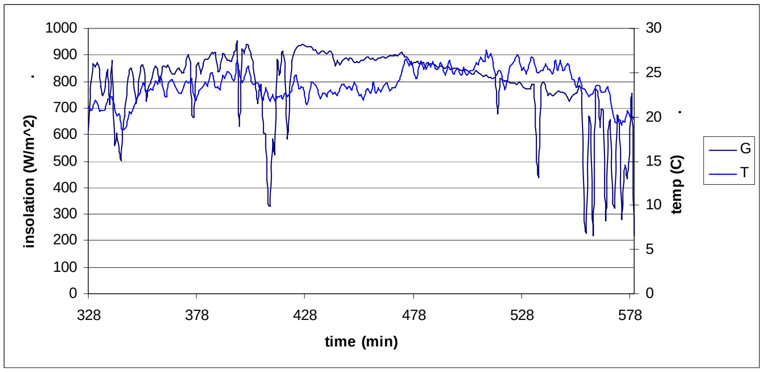

Figure 5.7 – March 19th 2007 SLO Insolation and Temperature

The plot of Figure 5.8 shows the battery status measurements taken by the SuPER status system on the 19th of March. The motor was run from 11:30 to 12:30.

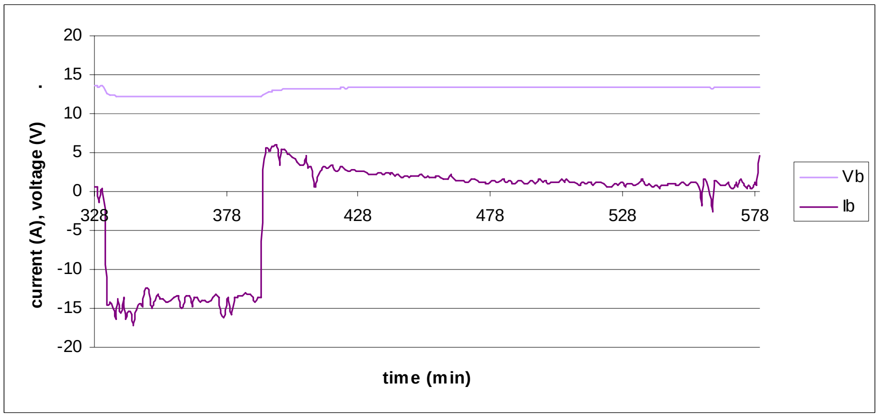

Figure 5.8 – March 19th 2007 Motor Operation Measurements

The insolation and temperature data taken during the day are fed into the Simulink simulation. The resulting estimated voltages and currents are shown in Figure 5.9.

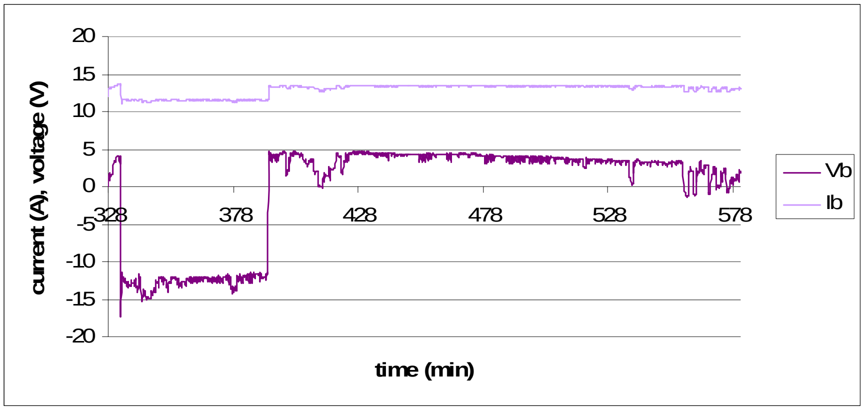

Figure 5.9 – March 19th 2007 Motor Simulation

Much of the "noise" that appears in the simulation plots is largely due to the coarse duty cycle resolution of 2.5%. Improved resolution, which would require greater simulation time, would result in much more accurate levels. However, the general trends over time can clearly be seen. These are very promising results, in spite of the fact that we do not have a proper model for the Outback MX60 converter or its control algorithm.

Figure 5.10 shows, for the same time frame, the battery SOC as predicted by the charge estimation code running on the laptop as compared to the simulation SOC estimate.

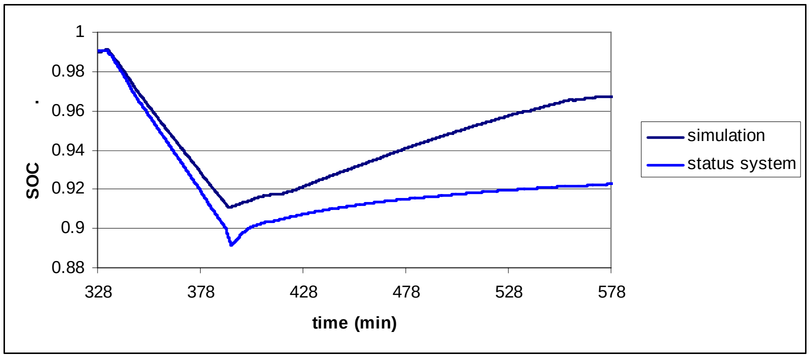

Figure 5.10 – March 19th 2007 SOC Estimates

In reality, the measured battery Voc taken 24 hours after operation was suspended indicated a fully charged battery. In consistently being conservative while tweaking the battery model, it is possible that the battery's capabilities have been underestimated – good news in terms of the viability of SuPER. However, it was also observed that the simulation tends to predict higher currents and voltages than the prototype battery actually experiences. Perfecting the model will require time and careful attention to detail.

Another motor test was performed on the 29th of March, conditions for which are found in Figure 5.11.

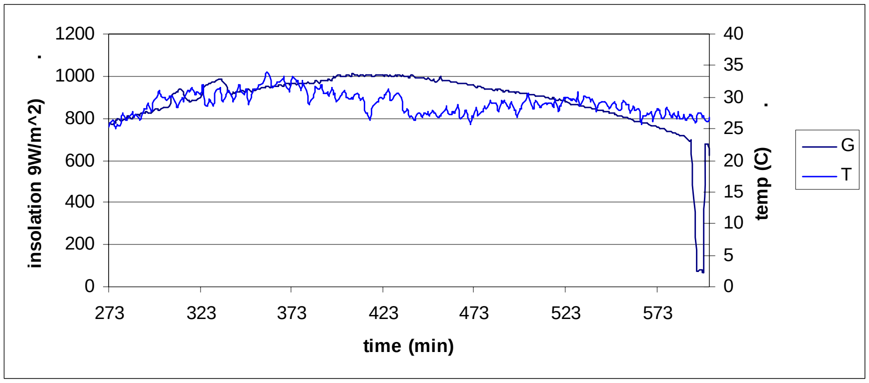

Figure 5.11 – March 29th 2007 Insolation and Temperature

This time the motor is run from 12:30 to 13:30, which is the peak insolation period for this time of year in San Luis Obispo, and the system measurements are shown in Figure 5.12.

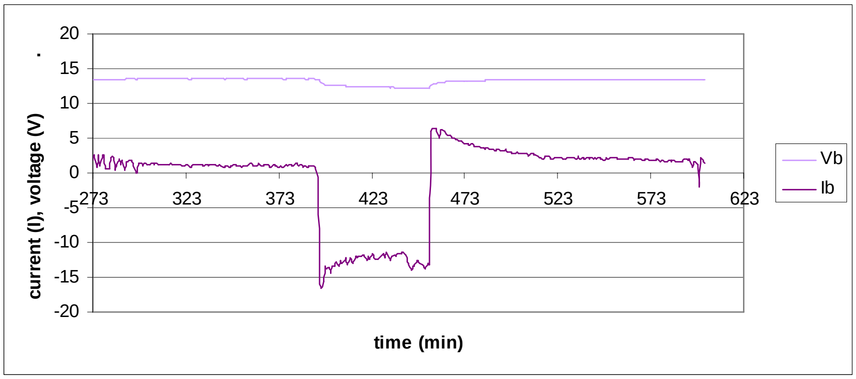

Figure 5.12 – March 29th 2007 Motor Operation Measurements

It is probable that the arc in the battery current while the motor was running is due to the dynamometer torque unexplainably creeping downwards. Figure 5.13 shows the same scenario in simulation.

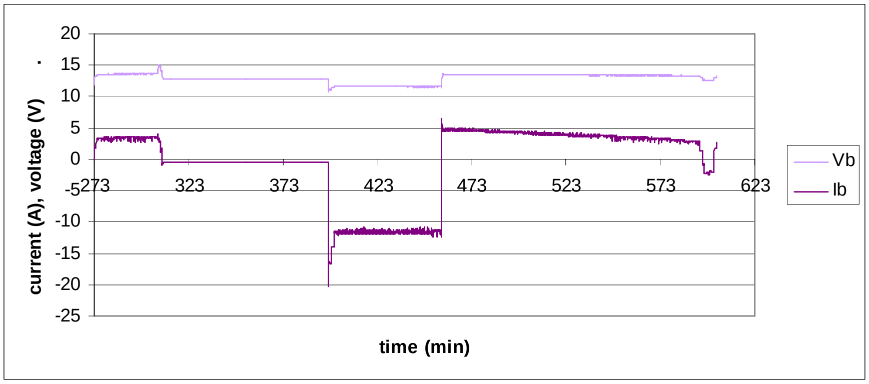

Figure 5.13 – March 29th 2007 Motor Simulation

Again the battery V_{oc} was found the next day to indicate a fully charged battery. We can only conclude that when starting motor operation with a full battery, there is plenty of available solar power to recharge the battery promptly whether the motor is powered an hour before peak insolation or during peak insolation. Future studies will adjust the battery model accordingly and may then take into account cloudy periods that force the battery to begin succeeding days with less than a full charge.

5.3 Multi-Load Scenarios

With the simulation, we can consider a variety of load scenarios over lengthy periods of time and view the ultimate effect on the battery. In this first example we run all five loads every day: television (two hours), cooler (1.67 hours), lights (three hours), laptop (14 hours), and motor (one hour). Again, the summer insolation data from Colorado will be utilized. Figure 5.14a shows the load activation schedule for two days, which places a demand of 1,833Wh on the array and battery. Note that in all of these examples, the two figures share the same time index.

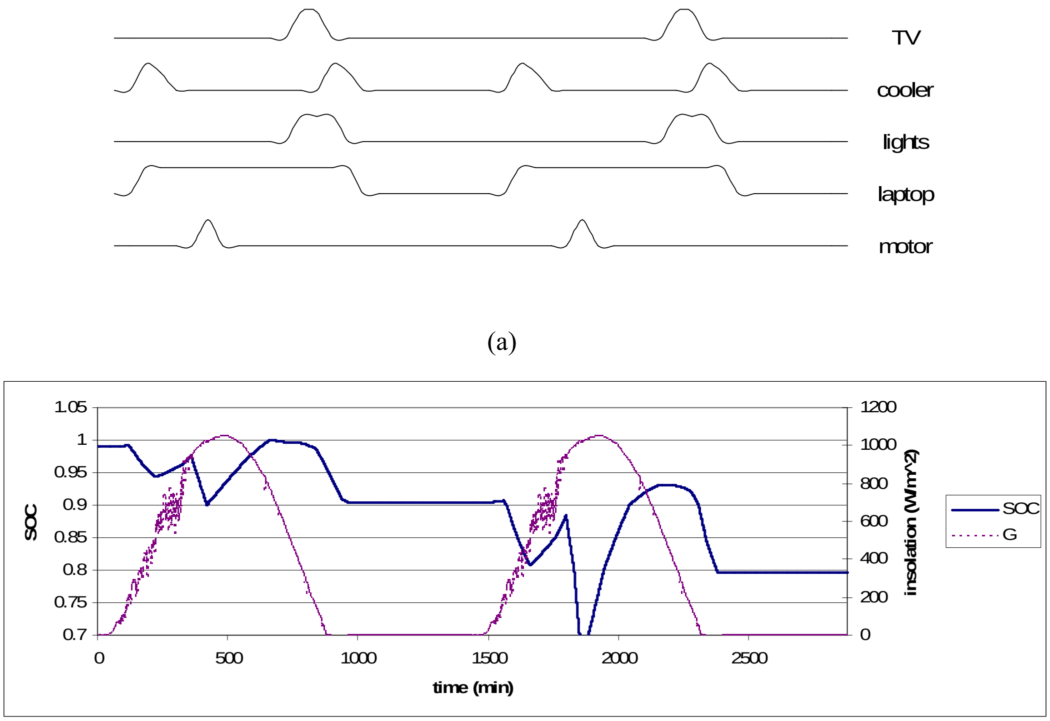

(a)

(b)

Figure 5.14 – Five Load / Two Day Scenario One: a) Load Schedule b) SOC Estimation

Figure 5.14b shows that in this case the battery SOC will clearly decline each day. Perhaps the problem can be remedied by operating the motor only every other day. Figure 5.15a gives the load schedule for a two-day new scenario, in which power needs are reduced to 1,583Wh for the two day period.

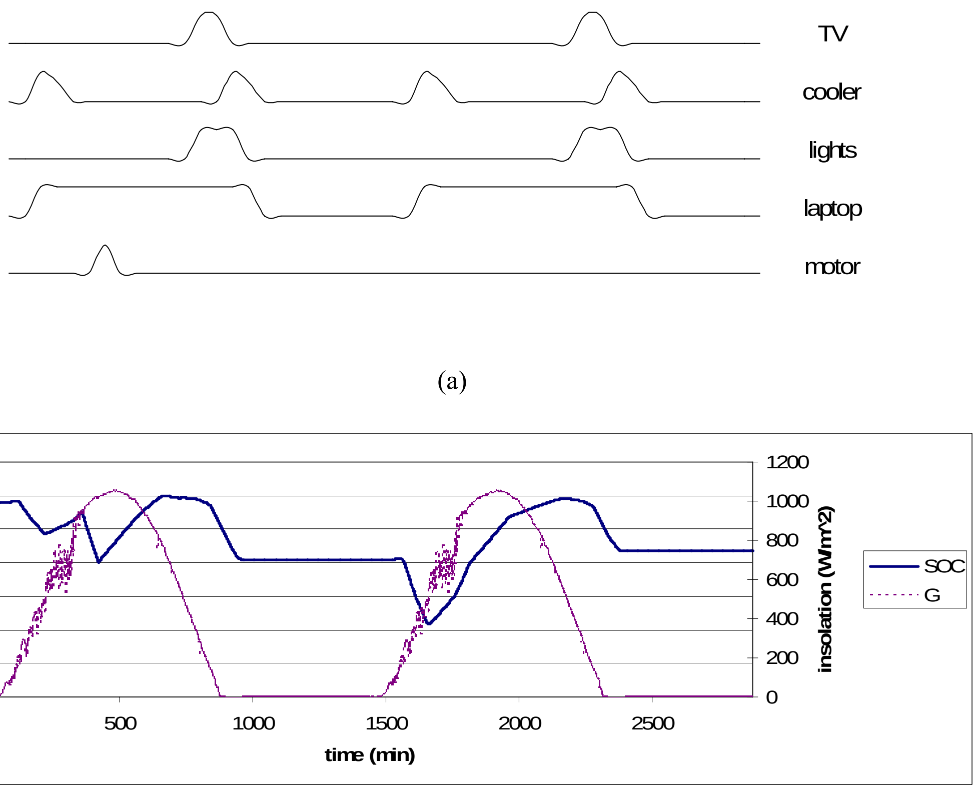

(a)

(b)

Figure 5.15 – Five Load / Two Day Scenario Two: a) Load Schedule b) SOC Estimation

Operating the motor only every other day results in a more sustainable operation scenario, as the second day allows for some recovery for the battery; however it can be seen (Figure 5.16b) that the SOC at the end of the second day is much lower than the initial SOC. This is cause for concern if the motor is required to run on the third day.

In this final case, all cooler operation is halted and the motor is operated every day for one hour. All other loads are unchanged, with the needed energy now reduced to 1,399Wh. See Figure 5.17 for the schedule and results.

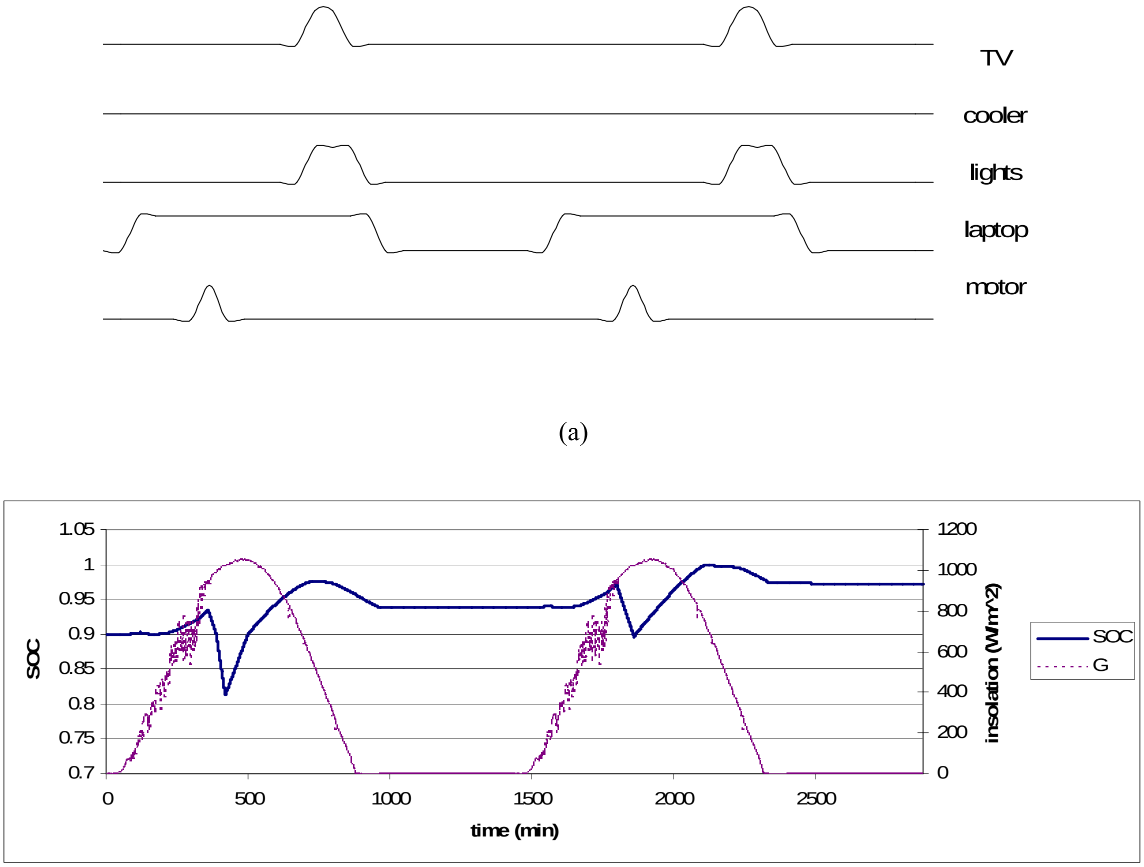

(a)

(b)

Figure 5.16– Four Load / Two Day Scenario Three: a) Load Schedule b) SOC Estimation

The battery is now able to build charge on sunny days, which will allow some reasonable DOD to occur on cloudy days without significant repercussions to battery lifetime.

5.4 Power Losses

Systems whose characteristics include high currents traversing non-trivial distances face losses due to resistances in components such as cables and switches. SuPER is no exception. Model development has not reached the point where sophisticated representations for these sinks have been developed. Using the measured voltage drop and current flow between the converter and battery, and between battery and loads, some idea of losses can be estimated. Consider a simple resistive loss model (Figure 5.18) where R1 and R2 represent switch and cable resistances between subsystems.

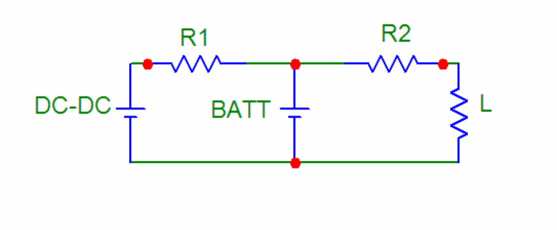

Figure 5.17 – Simple Resistive Loss Model

Some data has been gathered on system losses under multiple load scenarios. Figure 5.19 shows power levels for various system components while running a 70W load for 250 minutes. P3 represents the power consumed by the load.

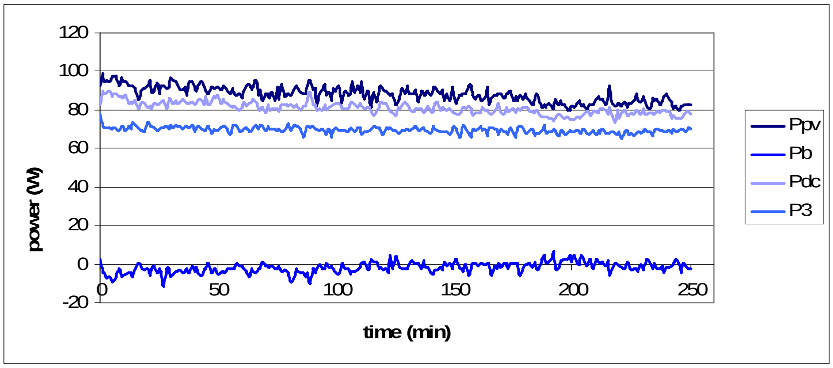

Figure 5.18 – System Power Levels, 70W Load on CKT #3

Using this information, we can capture an idea of the efficiency of the Outback MX60 converter at certain power input levels. Figure 5.20 shows how the efficiency rises as the input power drops.

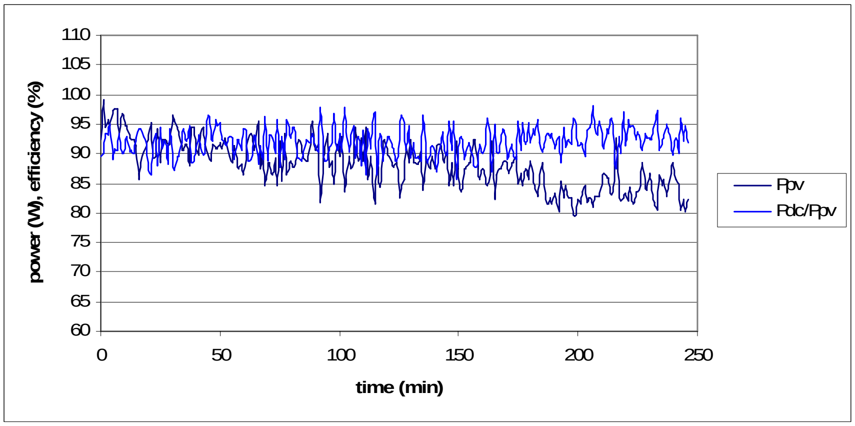

Figure 5.19 – PV Power and Converter Efficiency

In fact, with input power of about 50W or less, converter efficiency is near 100%. Some of these phenomena uncovered while exploring status system information will certainly attract further investigation in the near future. Averaging chunks of this data, we can conjecture a bit as to the behavior of the elements involved in these losses, assuming the given simple loss model (see Table 5.1).

Table 5.1 – Estimates for Values of Loss Contributive Elements

Characteristic	PV Power	Value
MX60 efficiency	90W	~92%
MX60 efficiency	80W	~94%
MX60 efficiency	<= 50W	~100%
R1	90W	.031 Ω
R1	80W	.029 Ω
R1	50W	.024 Ω
R2	90W	.038 Ω
R2	80W	.055 Ω
R2	50W	.048 Ω

There is a clear indication that R1 will increase as the PV array power increases. The losses are greatly dependent on the amount of power being distributed, as resistive losses are proportional to the square of the current. R2 is more difficult to qualify.

The 10-gauge wire connecting the DC-DC converter output to the battery and loads runs approximately twelve feet in length; twelve feet of 10-gauge wire offers about .02 Ω of resistance. Presupposing that we can attribute some of the measured losses to the wiring, but not all, this value seems to corroborate what has been observed. This first generation Simulink model has had a collective .04Ω resistance introduced on the converter and battery output, a value chosen to lie between the calculated wire resistance and the estimated simple loss model resistances representative of the uncertainty in the true sources of these losses.

Future work on SuPER will need to examine these effects. Analysis should be made towards the end of discovering where exactly these losses occur, and how they relate to the voltage and current. Potentially, the highest sources of loss may be the cables, battery inefficiency, and switches. Also, the various sensor boards will consume some power. A possibility worth investigating would be increasing the voltage and decreasing the current on the load side of the converter, perhaps by going to a 24V battery. Another factor for inconsistency to keep in mind is that only the PV array block takes temperature into account for calculating power output. In reality, the battery and converter subsystems will also be dependent upon the temperature. Improvements can be made to factor temperature levels into model behavior.

Chapter 6: Conclusion

6.1 Achievements

The loop still has not been closed on the Phase 1 system, as we set out to do in the fall of 2006. It was necessary to adjust some of the team goals to better fit the available human resources. Focus was turned toward simulating the entire system in software. After months of effort, the first generation Simulink model presented herein has shown heartening results. The SuPER team is now equipped with a viable "first-order" Simulink model of the entire system. Adjustable parameters will enable the simulation to provide greater service as a virtual representation of the SuPER prototype in the near future. The model can then be easily modified to allow for

- increasing the PV array size
- introducing more efficient PV array technology
- introducing new battery models
- adding new loads
- better representation of power losses in the system (heat, etc)
- development of adaptive control

The status and control software structure is now ready for the future integration of the DC-DC converter, although some modifications may be necessary depending upon the manner in which the converter will be controlled. The Phase 0 prototype has been put through its paces, as all five developmental loads have been tested and characterized. With the assistance of undergraduate students, great progress on other system aspects such as LED lighting and high-current PCB manufacturing has been made. These simulation tools and other development processes that have been established will facilitate the achievement of SuPER's goals for the next few years. We are well on our way.

6.2 Reflection on System Sensitivities

Despite some hardware setbacks, the SuPER project has arrived at a key point in the development process. Many of the limitations of the design have been uncovered and assessed, and work identified for years ahead. The battery turns out to be one of the most difficult problems because of the complexities involved in accurately modeling it. In order to create a system that will be cost effective, we desire the battery to last as long as possible. To create control software that will optimize battery life, intimate knowledge of the battery's characteristics must be obtained. There are other battery technologies that are more reliable and more easily characterized than the VRLA variety, but suffer from other limitations such as stunted storage capacity. Improvements in electrical energy storage technologies will hopefully usher SuPER towards greater viability.

Besides optimizing battery life, there are two fundamentally important challenges that will confront the future generations of SuPER project collaborators: lowering system cost and finding ways to utilize power more efficiently. SuPER's success will of course rely on advances in PV cell technology as well. The goal of the SuPER project is that when that day arrives, new PV cells and batteries can simply be inserted into an already-proven digitally-controlled distribution system. To justify the cost of the new cells and batteries, the balance of the SuPER infrastructure must be as economical and efficient as possible.

Table 6.1 outlines the project costs to date. Loads are part of the development cost, but are not part of the $500 target for the end user system cost.

Table 6.1 – SuPER Development Costs to Date

Infrastructure	**Unit**	**Cost**
	Dell Inspiron B120 Laptop Lind Electronics DC-DC Converter BP 150SX Solar Panel 12V Gel VRLA Battery 98 Ah (20h) NI USB-6009 DAQ Devices Wiring, breakers, connectors, etc. PCBs	$450 $140 $750 $150 $420 $460 $400
Loads	GPX Portable 5" television Coleman 12V DC Refrigerator LED Lights (x4) Dayton DC motor	$15 $90 $70 $275

These costs total $2,074 for the SuPER infrastructure, with nearly $3,000 in developmental expenditures up to this point. One of the key cost-cutting measures will be the replacement of the laptop and NI DAQ devices at the core of the status and control system. Eventually we would like to see a low-power FPGA take on all status and control duties. This alone would reduce costs by nearly $1,000. As the system takes shape, wiring and parts costs will be reduced significantly, and PCB manufacturing processes will have the same effect. Certainly the battery and PV array will be the most costly single components of the system, and hence SuPER's anticipation of future breakthroughs on these technologies.

6.3 Recommendations

The need to finalize the Phase 1 system by completing integration of the DC-DC converter cannot be overemphasized. The Outback MX60 is strictly a temporary solution, and much of the Simulink model's future effectiveness as a virtual system modeling tool and test bed will depend upon the converter. This is the single most important step for furthering SuPER progress.

The SuPER team may want to remove confusion by using the Celsius scale for all future cooler load work. Fahrenheit has been used to this point because the manufacturer chose to describe the cooler characteristics on that scale.

The losses inherent in the prototype infrastructure ought to be investigated. There is nothing that will restrict further progress on SuPER in this matter, but achieving the highest possible efficiency may require a future redesign of the distribution bus side of the system.

The VRLA battery storage is another topic of interest whose characteristics may also contribute to some of the system losses; however, it is not entirely clear how much more effort should be expended toward properly modeling the battery. Certainly some time should be spent towards including battery temperature as one of the model inputs, but despite the large amounts of research done on these types of batteries they are still destined to be difficult to model accurately. A decision should be made in the near future on how much more time and money should be invested into the current battery and model. As for incorporation of the battery temperature measurement, it appears that thermocouple technology is the best bet for reading the temperature on the battery itself.

Bibliography

[1] Harris, James G. *White Paper for Sustainable Power for Electrical Resources – SuPER.* July 15,2005. <http://www.ee.calpoly.edu/~jharris/research/super_project/white_paper_susper.pdf>.

[2] Tal, Eran. "SuPER System Prototype Design and Implementation." Master's thesis, California Polytechnic State University, 2006.

[3] *Trends in Atmospheric Carbon Dioxide*. Chart. National Oceanic and Atmospheric Administration, 2007. <http://www.esrl.noaa.gov/gmd/ccgg/trends/>

[4] "Venture Capitalists Embrace Solar Energy". MSNBC 28 December 2005. <http://www.msnbc.msn.com/id/10625903>

[5] Mills, Evan. "The Specter of Fuel Based Lighting". *Science* 27 May 2005: 1263-1264.

[6] Sharaf, A.M. and A.R.N.M. Raez Ul Haque. "A Low Cost Stand Alone Photovoltaic Scheme for Motorized Hybrid Loads". IEEE Proceedings of the 36th Southeastern Symposium on System Theory, 2004.

[7] Chiang, S. J., K. T. Chang, and C. Y. Yen. "Residential Photovoltaic Energy Storage System." IEEE Transactions On Industrial Electronics, Vol. 45, No. 3, June 1998

[8] Vasquez, Gustavo. "Data Acquisition and Sensor Circuits for the SuPER Project". Senior Project report, California Polytechnic State University, 2006.

[9] Apogee Instruments, Inc. *Silicon Pyranometer Specifications.* Online Retailer. <http://www.apogee-inst.com/pyr_spec.htm>

[10] Frohlich, Claus. "Construction of a Composite Total Solar Irradiance (TSI) Time Series from 1978 to Present". PMOD/World Radiation Center, May 2006.

[11] Belov, I.M., M.P.Volkov, and S.M.Manyakin. "Optimization of Peltier Thermocouple Using Distributed Peltier Effect". 18th International Conference on Thermoelectrics, 1998.

[12] Zukowski, Joey. Senior Project report, California Polytechnic State University, 2007.

[13] Allbatteries UK Ltd. *Charging Lithium-ion Batteries.* Online Retailer. <http://www.powerpacks-uk.com/Charging%20Li-ion%20Batteries.htm>.

[14] Cao, Jennifer. "SuPER Project Wiring and Protection System". Senior Project report, California Polytechnic State University, 2006.

[15] East Penn Manufacturing Inc. *Valve Regulated Lead Acid Technical Manual*. Technical Manual, 2004.

[16] Witts, Joseph. "Using Ultra Capacitors for Energy Storage in Cal Poly's SuPER Project". Senior Project report, California Polytechnic State University, 2007.

[17] Vairamohan, Baskar. "State of Charge Estimation for Batteries". Master's Thesis, University of Tennesee, 2002.

[18] Duryea, Shane, Syed Islam, and William Lawrence. "A Battery Management System for Stand-Alone Photovoltaic Energy Systems". IEEE Industrial Applications Magazine, May/June 2001.

[19] Castaner, Luis and Santiago Silvestre. *Modeling Photovoltaic Systems*. John Wiley & Sons Ltd, 2002.

[20] Den Herder, Tyson. "Design and Simulation of Photovoltaic SuPER System Using Simulink". Senior Project report, California Polytechnic State University, 2006.

[21] Fasih, Ahmed. "Modeling and Fault Diagnosis of Automotive Lead-Acid Batteries." Master's thesis, The Ohio State University, 2006.

[22] Outback Power Systems, Inc. *MX60 PV MPPT Charge Controller*. Installation and User's Manual, 2005.

[23] Outback Power Systems, Inc. *MX60 Specifications*. Datasheet, 2005.

[24] Guno, Thaddeus, Koosh Shah and Kunal Shah. Senior Project report, California Polytechnic State University, 2007.

[25] Casanova, Robert and Joe Shein. "SuPER DC-DC Buck Converter". Senior Project report, California Polytechnic State University, 2007.

[26] National Instruments Corp. *User Guide and Specifications USB 6008/6009*. Technical Manual, 2005.

[27] National Instruments Corp. *NI-DAQmx Base 2.x C Function Reference Help*. Technical Manual, 2005.

[28] Oi, Aki. "Design and Simulation of Photovoltaic Water Pumping System". Master's thesis, California Polytechnic State University, 2005.

[29] Taufik. *A Crash Course in Switching Regulators*. Slide Presentation Notes, 2006.

[30] East Penn Manufacturing Inc. *Absorbed Glass Mat Series*. Datasheet, 2003.

[31] The MathWorks, Inc. *MATLAB User Guide*. Technical Manual, 2005.

Appendix A: NI-DAQmxBase 2.1 API Function List

Function Purpose	Function Names
Task Configuration/Control	DAQmxBaseClearTask DAQmxBaseCreateTask DAQmxBaseIsTaskDone DAQmxBaseLoadTask DAQmxBaseResetDevice DAQmxBaseStartTask DAQmxBaseStopTask
Create Analog Input Channels	DAQmxBaseCreateAIThrmcplChan DAQmxBaseCreateAIVoltageChan
Create Analog Output Channel	DAQmxBaseCreateAOVoltageChan
Create Digital Input Channels	DAQmxBaseCreateDIChan
Create Digital Output Channels	DAQmxBaseCreateDOChan
Create Counter Input Channels	DAQmxBaseCreateCIPeriodChan DAQmxBaseCreateCICountEdgesChan DAQmxBaseCreateCIPulseWidthChan
Create Counter Output Channels	DAQmxBaseCreateCOPulseChanFreq
Timing	DAQmxBaseCfgSampClkTiming DAQmxBaseCfgImplicitTiming
Triggering	DAQmxBaseDisableStartTrig DAQmxBaseCfgDigEdgeStartTrig DAQmxBaseCfgAnlgEdgeStartTrig
Reference Trigger	DAQmxBaseCfgAnlgEdgeRefTrig DAQmxBaseCfgDigEdgeRefTrig DAQmxBaseDisableRefTrig
Read Functions	DAQmxBaseReadAnalogF64 DAQmxBaseReadBinaryI16 DAQmxBaseReadCounterF64 DAQmxBaseReadCounterScalarF64 DAQmxBaseReadCounterScalarU32 DAQmxBaseReadCounterU32 DAQmxBaseReadDigitalScalarU32 DAQmxBaseReadDigitalU32 DAQmxBaseReadDigitalU8
Write Functions	DAQmxBaseWriteAnalogF64 DAQmxBaseWriteDigitalU8 DAQmxBaseWriteDigitalU32 DAQmxBaseWriteDigitalScalarU32
Internal Buffer Configuration	DAQmxBaseCfgInputBuffer
Error Handling	DAQmxBaseGetExtendedErrorInfo

Appendix B: Status Data Extraction Macro for Excel

There are two versions of the macro, one each for TIME_FACTOR = 15 and TIME_FACTOR = 30. They are both found in *super_status_macros.xls.* This macro performs a moving average with a window of width five, and then downsamples the result by a factor NUM_TO_OUTPUT * 60 / T_{ss} (currently 150) to supply one sample per minute of run time. Upon running the macro, the data appears in columns S through AE. All sensor data except the converter and battery temperatures are assessed. The macro can easily be edited to include them if necessary.

Appendix C: PIC Serial Communication Protocol

This protocol was originally created to facilitate testing over a Hyper Terminal interface, but later adapted to the C code. It was designed for the 16-series, but also services the 18-series.

Type (send) M<value> to set 8 highest-order bits of the duty cycle register.
Type (send) L<value> to set 2 lowest-order bits of the duty cycle register.
The PIC will echo back an exclamation point '!' to confirm receipt.
The highest-order bits range is integers 55 – 155, for a duty cycle of 0 – 100% (e.g. an integer 65 will result in a DC of 10%).
There are only four possible values for the lowest-order bits, 0-3.
Use chars '0', '1', '2', '3' (integers 48, 49, 50, 51) to fine-tune the duty cycle.

For example, to get a duty cycle of 17.25%, type 'MHL1' in HT. This will echo back as 'MH!L1!'. To get a duty cycle of 45.75%, type 'MdL3'. This will echo back as 'Md!L3!'. In C, simply transmit four bytes: 'M' 72 'L' 49 for the first case, or 'M' 100 'L' 51.

Any character entered that is not an M or L or not prefaced by M or L will be ignored and simply echo back followed by an '!'.

Appendix D: C-MEX S-function Code

D.1 PV Array S-function Code

```
// function PV(block)
// % wrapper S-function around Aki's pv array model
// % in: G (irradiance, KW/m^2), TaC (temp, deg C), Vpv
// % out: Ipv
// %
// %
// %  Adapted to C by Tyler Sheffield 2/14/06
// %////////////////////////////////////////////////////////////////


double Ia_new; //= bp_sx150s(Vs,G,TaC);
double Va = Vpv[0];
double ac = 0.8;       // attenuation coefficient based on observed max power
int j;


// function Ia = bp_sx150s(Va,G,TaC)
// % function bp_sx150s.m models the BP SX 150S PV module
// % calculates module current under given voltage, irradiance and temperature
// % Ia = bp_sx150s(Va,G,T)
// %
// % Out: Ia = Module operating current (A), vector or scalar
// % In: Va = Module operating voltage (V), vector or scalar
// % G = Irradiance (1G = 1000 W/m^2), scalar
// % TaC = Module temperature in deg C, scalar
// %
// % Written by Akihiro Oi 7/01/2005
// % Revised 7/18/2005
// %/////////////////////////////////////////////////////////////////////////////
// % Define constants
double k = 1.381e-23; //% Boltzmann’s constant
double    q = 1.602e-19; //% Electron charge
// % Following constants are taken from the datasheet of PV module and
// % curve fitting of I-V character (Use data for 1000W/m^2)
double n = 1.62; //% Diode ideality factor (n),
// % 1 (ideal diode) < n < 2
double Eg = 1.12; //% Band gap energy; 1.12eV (Si), 1.42 (GaAs),
// % 1.5 (CdTe), 1.75 (amorphous Si)
double Ns = 72; //% # of series connected cells (BP SX150s, 72 cells)
double TrK = 298; //% Reference temperature (25C) in Kelvin
double Voc_TrK = 43.5 /Ns; ///% Voc (open circuit voltage per cell) @ temp TrK
double Isc_TrK = 4.75; //% Isc (short circuit current per cell) @ temp TrK
double a = 0.00065; //% Temperature coefficient of Isc (0.065%/C)
// % Define variables
double TaK = 273 + TaC[0]; //% Module temperature in Kelvin
double Vc = Va / Ns; //% Cell voltage
// % Calculate short-circuit current for TaK
double Isc = Isc_TrK * (1 + (a * (TaK - TrK)));
// % Calculate photon generated current @ given irradiance
double Iph = G[0] * Isc;
// % Define thermal potential (Vt) at temp TrK
double Vt_TrK = n * k * TrK / q;
// % Define b = Eg * q/(n*k);
double b = Eg * q /(n * k);
// % Calculate reverse saturation current for given temperature
double Ir_TrK = Isc_TrK / (exp(Voc_TrK / Vt_TrK) -1);
double Ir = Ir_TrK * pow((TaK / TrK),(3/n)) * exp(-b * (1 / TaK -1 / TrK));
// % Calculate series resistance per cell (Rs = 5.1mOhm)
double dVdI_Voc = -1.0/Ns; //% Take dV/dI @ Voc from I-V curve of datasheet
double Xv = Ir_TrK / Vt_TrK * exp(Voc_TrK / Vt_TrK);
double Rs = - dVdI_Voc - 1/Xv;
// % Define thermal potential (Vt) at temp Ta
double Vt_Ta = n * k * TaK / q;
```

```
// % Ia = Iph - Ir * (exp((Vc + Ia * Rs) / Vt_Ta) -1)
// % f(Ia) = Iph - Ia - Ir * ( exp((Vc + Ia * Rs) / Vt_Ta) -1) = 0
// % Solve for Ia by Newton's method: Ia2 = Ia1 - f(Ia1)/f'(Ia1)
Ia_new = 0; //% Initialize Ia_new with zero

// % Perform 5 iterations
for (j=1; j<=5; j++) {
    Ia_new = Ia_new - (Iph - Ia_new - Ir * ( exp((Vc + Ia_new * Rs) / Vt_Ta) -1)) / (-1 -
Ir * (Rs / Vt_Ta) * exp((Vc + Ia_new * Rs) / Vt_Ta));
}

Ipv[0] = Ia_new*ac;
```

D.2 Control S-function Code

```
// control_plus_src.c
// function control(block)
// % function to execute MPPT via pwm duty cycle of pv module and control load
// % switches (1 == bulk charge, 2 == float charge)
// % in: Vpv, Ipv, Vb, charge_mode
// % out: DC, DCprev, Pa
// %
// % Written by Tyler Sheffield 12/10/06
// % Adapted to C by Tyler Sheffield on 2/14/06
// %/////////////////////////////////////////////////////////////////

//     % Define variables and initialize
double C = 0.025;        //% Step size for duty cycle change 2.5%

//     % Calculate new Pa
double Pa_new = Vpv[0] * Ipv[0];

//  deltaPa adjustment offset
double dpoffset = 0;

//     pass-through values
double DCnew = DC[0];
charge_mode_out[0] = charge_mode[0];

if (charge_mode[0] == 1 && Pa_new < 3)        // low power state, always go up
  DCnew = DC[0] + C; //% Increase DC

else if (charge_mode[0] == 1 && Vb[0] < 13.7){   //        % bulk charge case
  //           % P&O Algorithm starts here
  double deltaPa = Pa_new - Ppv[0] + dpoffset;
  count[0] = 0;  // reset float mode counter
  if (deltaPa >= 0) {   //      % keep going
      if (DC[0] > DCprev[0])
          DCnew = DC[0] + C; //% Increase DC
      else
          DCnew = DC[0] - C; //% Decrease DC
  }
  else if (deltaPa < 0) {   //  % go opposite
      if (DC[0] > DCprev[0])
          DCnew = DC[0] - C; //% Decrease DC
      else
          DCnew = DC[0] + C; //%Increase DC
  }
  else
      DCnew = DC[0]; //% No change
} //elseif

else if (charge_mode[0] == 1 && Vb[0] >= 13.7) {
 count[0] = count[0]+1;
 if (count[0] > 1) {    // must read 13.7 twice to enter float mode
```

```
     charge_mode_out[0] = 2;     //% change to float mode
     DCnew = DC[0] - C;      //% Decrease DC
 } //if
} //elseif

else if (charge_mode[0] == 2 && Vb[0] >= 13.4)    //% move towards disconnect
 DCnew = DC[0] - C;      //% Decrease DC

else if (charge_mode[0] == 2 && Vb[0] < 12.7) {    //% reenter bulk mode (must avoid
thermal runaway)
 charge_mode_out[0] = 1;
 //DCnew = DC[0] + C; //% Increase DC
}

if (DCnew < 0)
 DCnew = 0;
if (DCnew > 1.0)
  DCnew = 1.0;
//        % Update history
DCprev[0] = DC[0];
DCout[0] = DCnew;
Ppv[0] = Pa_new;
```

D.3 Switch Control S-function Code

```
// function swcontrol(block)
//
// % function to control load switches based on scenario
// %
// % all ton/toff values are in minutes of the day
// % Ts = one minute
// % in: scenario number, system time
// % out: switches[5]
// %
// % Written by Tyler Sheffield 2/7/07
// %////////////////////////////////////////////////////////////////

#define INSTANCES 8          // number of on/off pairs for each load
#define INA 5000        // defines inactive parameter (never reached in time)
int i=0,j=0;
double table[5][INSTANCES];            // set up time table
double stime1000 = stime[0]*1000;
//int stime_int = (int) stime1000;   // this skews the value for some reason

// %         [
  // %         tv_ton            tv_toff ;
  // %         cooler_ton        cooler_toff ;
  // %         light_ton         light_toff  ;
  // %         laptop_ton        laptop_toff  ;
  // %         motor_ton         motor_toff  ;
  // %         ]
if (((int)scenario[0]) == 0) {
   table[0][0]=INA;table[0][1]=INA;  table[0][2]=INA;table[0][3]=INA;
table[0][4]=INA;table[0][5]=INA;      table[0][6]=INA;table[0][7]=INA;
   table[1][0]=INA;table[1][1]=INA;  table[1][2]=INA;table[1][3]=INA;
table[1][4]=INA;table[1][5]=INA;      table[1][6]=INA;table[1][7]=INA;
   table[2][0]=60;table[2][1]=120;     table[2][2]=INA;table[2][3]=INA;
table[2][4]=INA;table[2][5]=INA;   table[2][6]=INA;table[2][7]=INA;
   table[3][0]=0;table[3][1]=120;  table[3][2]=720;table[3][3]=INA;
table[3][4]=INA;table[3][5]=INA;        table[3][6]=INA;table[3][7]=INA;
   table[4][0]=INA;table[4][1]=INA;  table[4][2]=INA;table[4][3]=INA;
table[4][4]=INA;table[4][5]=INA;        table[4][6]=INA;table[4][7]=INA;
}
if (((int)scenario[0]) == 1) {
   table[0][0]=INA;table[0][1]=INA;  table[0][2]=INA;table[0][3]=INA;
table[0][4]=INA;table[0][5]=INA;      table[0][6]=INA;table[0][7]=INA;
   table[1][0]=0;table[1][1]=100;  table[1][2]=INA;table[1][3]=INA;
table[1][4]=INA;table[1][5]=INA;      table[1][6]=INA;table[1][7]=INA;
   table[2][0]=INA;table[2][1]=INA;     table[2][2]=INA;table[2][3]=INA;
table[2][4]=INA;table[2][5]=INA;   table[2][6]=INA;table[2][7]=INA;
   table[3][0]=0;table[3][1]=INA;  table[3][2]=INA;table[3][3]=INA;
table[3][4]=INA;table[3][5]=INA;        table[3][6]=INA;table[3][7]=INA;
   table[4][0]=INA;table[4][1]=INA;  table[4][2]=INA;table[4][3]=INA;
table[4][4]=INA;table[4][5]=INA;        table[4][6]=INA;table[4][7]=INA;
}
for (i=0;i<5;i++) {         // i is the load index
   for (j=0;j<8;j++) {     // j is the time value index
       if (fabs(table[i][j] - stime1000) < .1 ) {  // double type adjustment
           switches[i] = !switches[i];              // flip switch
           break;
       } //if
   } //for
} //for
```

D.4 Battery S-function Code

```
// batt_voltage_src.c
// % VRLA battery model
// % in: SOC1 (initial SOC), I1
// % out: SOC2, Vbat
//
//   Adapted to C by Tyler Sheffield 2/14/06
// %////////////////////////////////////////////////////////////////

// define constants
double SD = 4.34e-5; //%battery self-discharge rate (h^-1)
double SOCm = 1330; //%max. battery energy (Wh)
double ns = 6; //%number of 2V series cells
double SOC,ee,B;      // temp vars

// adjustable parameters
double k = .8; //%battery charge/discharge efficiency
double t = 0.0033334;    // time step constant (equal to block sample time converted to
real time)
// resistance model adjustment multipliers
double rd8=5,rc8=15,rd9=50,rc9=15,rd10=50,rc10=15;
// SOC coefficients
double phi8=2.174, phi9=1.43, phi10=.625;

if (fabs(I1[0]) > 2)            // high current case requires battery capacity adjustment
   SOCm = -179.68*log(fabs(I1[0])) + 1435.2;      // taken from Excel curve mapping

SOC2[0] = SOC1[0];
B = SOC2[0];        // line 75

if (SOC1[0] < .8) {             //% under 80% case
   if (I1[0] <= 0){          // % discharge mode
       V1[0] = (1.95 + .18*B)*ns;
       R1[0] = (.19 + .1037/(B-.14))*ns*rd8/SOCm;
   }
   else if (I1[0] > 0) {        // % charge mode
       V1[0] = (2 + .148*B)*ns;
       R1[0] = (.758 + .1309/(1.06-B))*ns*rc8/SOCm;
   }
    ee = ((k*V1[0]*I1[0] - SD*SOC2[0]*SOCm)*t) * phi8;
   SOC =  SOC2[0] + ee/SOCm;
   SOC2[0] = SOC;
} //if

else if (SOC1[0] >= .8 && SOC1[0] < .9)      {
   if (I1[0] <= 0){         // % discharge mode
       V1[0] = (1.95 + .18*B)*ns;
       R1[0] = (.19 + .1037/(B-.14))*ns*rd9/SOCm;  //real
   }
   else if (I1[0] > 0) {      //% charge mode
       V1[0] = (2 + .148*B)*ns;
       R1[0] = (.758 + .1309/(1.06-B))*ns*rc9/SOCm;
   }
   ee = ((k*V1[0]*I1[0] - SD*SOC2[0]*SOCm)*t) * phi9;
   SOC =  SOC2[0] + ee/SOCm;
   SOC2[0] = SOC;
} //else if

else if (SOC1[0] >= .9 && SOC1[0] < 1)   {
   if (I1[0] <= 0){           //% discharge mode
       V1[0] = (1.95 + .18*B)*ns;
                         R1[0] = (.19 + .1037/(B-.14))*ns*rd10/SOCm;
   }
   else if (I1[0] > 0){        //% charge mode
       V1[0] = (2 + .148*B)*ns;
        R1[0] = (.758 + .1309/(1.06-B))*ns*rc10/SOCm;
    }
 ee = ((k*V1[0]*I1[0] - SD*SOC2[0]*SOCm)*t) * phi10;
 SOC =  SOC2[0] + ee/SOCm;
 SOC2[0] = SOC;
} //else if

else if (SOC1[0] >= 1) {
 if (I1[0] <= 0){           //% discharge mode
     V1[0] = (1.95 + .18*B)*ns;
     R1[0] = (.19 + .1037/(B-.14))*ns*50/SOCm;
 }
 else if (I1[0] > 0){        //% charge mode
     V1[0] = (2.1 + .148*B)*ns;
     R1[0] = (.758 + .1309/(1.06-B))*ns*30/SOCm;
 }
 ee = ((k*V1[0]*I1[0] - SD*SOC2[0]*SOCm)*t) / 4;
 SOC =  SOC2[0] + ee/SOCm;
 SOC2[0] = SOC;
} //else if

Vbat[0] = V1[0] + I1[0]*R1[0];
```

D.5 Laptop S-function Code

```
// laptop_load_src.c
// function laptop_load(block)
// % laptop load battery management mimic
// % in: time in minutes, initial estimated battery SOC (0,1)
// % out: load select switches, new SOC
// %
// % Written by Tyler Sheffield 1/15/07
// %/////////////////////////////////////////////////////////////////

LSOCout[0] = LSOC[0];

// %         % new SOC calculation
//         mexPrintf("%lf\n",t[0]);
if (LSOCout[0] >= 1)
     LSOCout[0] = 1;
else
    {/* calculation of LSOC here*/}



 if (LSOCout[0] >= .9) {
     swH[0] = 0;
     swL[0] = 1;
 }
 else if (LSOCout[0] < .9) {
     swH[0] = 1;
     swL[0] = 0;
 }
```

D.6 Cooler S-function Code

```
// cooler_load_src.c
// function cooler_load(block)
// % cooler temperature calculation (works only for nearly constant ext temp)
// % in: initial interior temperature, power state, external temp
// % out: new internal temp
// %
// % Written by Tyler Sheffield 3/19/07
// %/////////////////////////////////////////////////////////////////

 // set to one minute equivalent sample time

   // 8 quarts water values
 double w_rate = .008; // warming rate deg/min
 double c_rate = .05; // cooling rate deg/min
 //double Tdiff[0] = eTemp[0] - iTemp1[0];

 if (state[0] == 0)
     iTemp2[0] = iTemp1[0] + w_rate;
 else if (state[0] == 1)
     iTemp2[0] = iTemp1[0] - c_rate;

 Tdiff[0] = eTemp[0] - iTemp2[0];
```

Appendix E: Choosing a Fixed-Step Solver

(extracted from [31])

When the Type control of the Solver configuration pane is set to fixed-step, the configuration pane's Solver control allows you to choose one of the set of fixed-step solvers that Simulink provides. The set of fixed-step solvers comprises two types of solvers: discrete and continuous.

The fixed-step discrete solver computes the time of the next time step by adding a fixed step size to the time of the current time. The accuracy and length of time of the resulting simulation depends on the size of the steps taken by the simulation: the smaller the step size, the more accurate the results but the longer the simulation takes. If you allow Simulink to choose the step size, Simulink sets the step size to the fundamental sample time of the model if the model has discrete states. This choice assures that the simulation will hit every simulation time required to update the model's discrete states at the model's specified sample times.

The fixed-step discrete solver has a fundamental limitation. It cannot be used to simulate models that have continuous states. If you attempt to use the fixed-step discrete solver to update or simulate a model that has continuous states, Simulink displays an error message. Thus, updating or simulating a model is a quick way to determine whether it has continuous states.

The continuous solvers employ numerical integration to compute the values of a model's continuous states at the current step from the values at the previous step and the values of the state derivatives. Simulink provides two distinct types of fixed-step continuous solvers: explicit and implicit solvers. Explicit solvers compute the value of a state at the next time step as an explicit function of the current value of the state and the state derivative, e.g.,

$$X(n+1) = X(n) + h * DX(n)$$

where X is the state, DX is the state derivative, and h is the step size. An implicit solver computes the state at the next time step as an implicit function of the state and the state derivative at the next time step, e.g.,

$$X(n+1) - X(n) - h*DX(n+1) = 0$$

This type of solver requires more computation per step than an explicit solver but is also more accurate for a given step size. The following table lists the available solvers and the integration techniques they use.

Solver	Class	Integration Technique
ode1	Explicit	Euler's Method
ode2	Explicit	Heun's Method
ode3	Explicit	Bogacki-Shampine Formula
ode4	Explicit	Fourth-Order Runge-Kutta (RK4) Formula
ode5	Explicit	Dormand-Prince Formula
ode14x	Implicit	Newton’s Method and Extrapolation

The integration techniques used by the fixed-step continuous solvers trade accuracy for computational effort. The table lists the solvers in order of the computational complexity of the integration methods they use from least complex (ode1) to most complex (ode5).

Choosing a Fixed-Step Continuous Solver

Any of the fixed-step continuous solvers in Simulink can simulate a model to any desired level of accuracy, given enough time and a small enough step size. Unfortunately, in general, it is not possible, or at least not practical, to decide a priori which solver and step size combination will yield acceptable results for a model's continuous states in the shortest time. *Determining the best solver for a particular model thus generally requires experimentation.*

Appendix F: Managing Scope Data

In the scope parameters dialogue box, click on the data history tab. Check the save data to workspace box and type the name of the struct wherein to store the data. At the format menu, select Structure with time. When the simulation has finished running, your data will be available in the MATLAB workspace, identified by the previously specified name. Double-click on the desired struct to open the array editor. To display the recorded scope data in a spreadsheet form, perform the following actions:

double-click the signals box
double-click the cell in the column corresponding to the desired signal
double-click the values box

The data can be plotted by selecting the column and clicking on the plot icon of the Array Editor toolbar. To export the data to Excel, run the m-file *storage_script.m*; it will take a moment for the data to be exported. The data is written to a file in the MATLAB *sim_waves* directory called *last_sim_data.xls*.

Setting the Scope Decimation Value

Open the scope window and click on the parameters button in the upper left. On the bottom is a text box marked Decimation. Enter the decimation value in the box.

Appendix G: Specifying Coverage Report Settings

(extracted from [31])

Coverage report settings appear in the Coverage Settings dialog, accessed through the Tools menu. Select the Generate HTML Report option to create an HTML report containing the coverage data generated during simulation of the model. A large part of using model coverage is specifying model coverage reporting options in the Coverage Settings dialog box.

Some of the data generated by the coverage report includes total simulation time, signal ranges, and subsystem complexity details. Note that activating coverage reporting may increase simulation time.

Appendix H: Improving Simulation Performance and Accuracy

(extracted from [31])

Simulation performance and accuracy can be affected by many things, including the model design and choice of configuration parameters. The solvers handle most model simulations accurately and efficiently with their default parameter values. However, some models yield better results if you adjust solver parameters.

Design Factors in Simulation Speed

Slow simulation speed can have many causes. Here are a few:

When a model includes a MATLAB function block or M-file S-function, the MATLAB interpreter is called at each time step, drastically slowing down the simulation. Using the math function block and C-MEX file S-functions will eliminate the need to invoke the interpreter.

Your model may include a Memory block. Using a Memory block causes the variable-order solvers (ode15s and ode113) to be reset back to order 1 at each time step. However, this does not appear to be an issue when using the fixed-step discrete solver.

The maximum step size may be too small. If you changed the maximum step size, try running the simulation again with the default value (auto).

Setting the relative tolerance too low can slow down the simulation. The default relative tolerance (0.1% accuracy) is usually sufficient. For models with states that go to zero, if the absolute tolerance parameter is too small, the simulation can take too many steps around the near-zero state values.

The problem might be stiff, but you are using a nonstiff solver. Try using ode15s.

Mixing sample times that are not multiples of each other causes the solver to take small enough steps to ensure sample time hits for all sample times. Smaller steps lead to longer simulation times.

Be sure to eliminate algebraic loops if possible. The solutions to algebraic loops are iteratively computed at every time step. Therefore, they severely degrade performance.

Appendix I: SuPER Prototype Operation

1. Ensure that all breakers are open.
2. Insert the hub cables into the laptop USB ports, followed by the NI DAQ device cables. Then insert the PIC cable into the open laptop port. The mouse cable should be inserted into the hub.
3. Power on the laptop (at this point running on its internal battery) and at the GRUB window choose the latest version of Red Hat.
4. Login using root:super1.
5. Open a shell and change directories (cd) to **/home/super1/pvpro/src** .
6. Close PV, converter and battery circuits by flipping the breakers marked PV, BATT and BUS.
7. Execute the software with the command **./contAcquireNChan** .
8. Flip the breakers as desired to power indicated loads.
9. To shut down the software, use ‘q’.
10. Shut everything down by opening all circuits at the breakers.

Appendix J: File README

```
SuPER Control System and Simulation README
Author:  Tyler Sheffield (tyler@galatix.com, 760.460.6880), 3/28/07
Last Update:   4/25/07

The files described in this readme are organized by directory, local to this CD.
File names have type extensions, while descriptions are bookended by +.
Directories on Linux are given in parentheses, if applicable.
Obsolete files (no longer used by the sim or master control) are marked with a ^.
Name placeholders, or wildcards if you will, are between ".
An * is a file type wildcard.

General Files:
/
+a collection of observations and important things to remember compiled during SuPER's
lifetime+
SuPER Master Documentation.doc

+the final thesis doc+
sheffield_thesis_4-25.doc

+the defense power point presentation+
SuPER Defense Presentation.ppt

+SuPER lab bulletin poster files+
nov 2 presentation (color rev).ppt
nov 2 presentation.ppt
nov 2nd presentation (alt 7).pdf


Laptop C Code:
c_code/
+All project code is found on the laptop in the directory file:/home/super1/.  The
pvpro/bin/, pvpro/etc/, and pvpro/lib/ folders

contain various utilities for the NI-DAQs to work properly.  The pvpro/include/ folder
has the file NIDAQmxBase.h, which is

included in all source that interfaces to the NI-DAQs.  Every time new interface code is
written, it should have these four

accompanying folders and their contents.  Each src/ folder contains the source code,
executable, and Makefile.  Simply type

'make' at the prompt while inside the src/ directory to compile the source.+

digpot/src/
(/home/super1/digpot/src/)

        +code for communicating over the 2-wire serial interface of the MAX5529 digital
pot+
        potcomm.c

cap/src/
(/home/super1/cap/src/)
        +code for the switches that control charging and discharging the ultracapacitor+
        cap.c

pvpro/src/
(/home/super1/pvpro/src/)

        +the brain of SuPER, where you will find main+
        contAcquireNChan.c

        +temporary storage file currently where the battery SOC is written+
        Super_Output.csv
```

```
pvpro/pno/
(/home/super1/pvpro/pno/)

        +PIC communication functions+
        commpic.c

        +stand-alone PNO code+
        pno.c^

        +PNO functions+
        pnopal.c


MATLAB:
draft_model/
        +these are the original Level 2 M-file S-functions+
        batt_voltage.m^
        control.m^
        control_plus.m^
        laptop_load.m^
        PV.m^
        swcontrol.m^

        +files generated by MATLAB from the S-function building blocks, upon build
command+
        "module_name"_c.c
        "module_name"_c.mexw32
        "module_name"_c_wrapper.c
        "module_name"_c.tlc

        +the storage files for the C-MEX S-function C code, not used by MATLAB+
        "module_name"_src.c

        +files associated with Aki's PV array model, and no longer directly used in
simulation+
        bp_sx50.m^
        bp_sx150s.m^
        PVmpp02.m^

        +script for writing all scope data out to Excel files (writes to
sim_waves/last_sim_data.xls)+
        storage_script.m

        +Tyson Den Herder's final model+
        system13a.mdl^

        +final SuPER model using C-MEX S-functions+
        super_c.mdl

        +other stages in the model development process, included in case of need as
reference+
        "model_name".mdl^


PIC Assembly:
pic/
+Note that there are other required files that come packaged with MPLAB, not supplied
here.  The mplab/ folder contains the MPLAB

setup files.  The diypack/ folder contains the MicroPro software.  The usbdrivers/ folder
contains drivers for the programmer

device. +

        +old PIC 16F877A code+
        pwm.asm^

        +current PIC 18F4320 code+
        pwm_18.asm

        +compiled hex generated by MPLAB, used to program PIC+
        pwm_18.hex

        +MPLAB project file (workspace)+
        SuperPWM_18.mcw

        +other files needed by the project file+
        SuperPWM_18.*

Assembly code editing, building and programming instructions:
        Open MPLAB
        Click File->Open Workspace
        Choose C:\Super\SuperPWM_18.mcw
        Edit pwm_18.asm as needed
        Click Project->Build All
        Connect the K128 programmer with PIC to the PC via a USB cable
        It may be necessary to check the COM port of the device with Device Manager
        Open MicroPro
        Click File->Port and enter the COM port of the USB programmer
        Check that the Chip Selector is correctly set
        Click File->Load
        Select the file C:\Super\pwm_18.hex
        Click Fuses and make sure the Oscillator pull-down menu is set to HS
        Click Program


Excel:
macros/
        +status system data extraction macros, see thesis Appendix B for usage
instructions+
        super_status_macros.xls


Data Files:
prototype_data/
        +status system data organized by date of operation+

sim_waves/
        +this folder is full of a variety of stored simulation results, just a couple
groups are identified here+

        +images of sim waves from first successful 24-hour period complete simulation run
(ran for 22 hours real time)+
        first all "name".bmp

        +simulation results of insolation and temp data taken from prototype motor
operation periods+
        march "date" motor.xls


All Others:
drawings/
        +MicroCap schematic drawings+
        "drawing name".cir

        +Visio drawings, flowcharts, etc.+
        "drawing name".vsd

experimental_data/
        +A repository for all other data and worksheets, etc. that had no place anywhere
else+
```